



1 **Size-resolved Composition and Morphology of Particulate**
2 **Matter During the Southwest Monsoon in Metro Manila,**
3 **Philippines**
4

5 Melliza Templonuevo Cruz^{1,2}, Paola Angela Bañaga^{1,3}, Grace Betito³, Rachel A. Braun⁴, Connor
6 Stahl⁴, Mojtaba Azadi Aghdam⁴, Maria Obiminda Cambaliza^{1,3}, Hossein Dadashazar⁴, Miguel
7 Ricardo Hilario³, Genevieve Rose Lorenzo¹, Lin Ma⁴, Alexander B. MacDonald⁴, Preciosa
8 Corazon Pabroa⁵, John Robin Yee⁵, James Bernard Simpas^{1,3}, Armin Sorooshian^{4,6}

9

10 ¹Manila Observatory, Quezon City 1101, Philippines

11 ²Institute of Environmental Science and Meteorology, University of the Philippines, Diliman, Quezon City 1101,
12 Philippines

13 ³Department of Physics, School of Science and Engineering, Ateneo de Manila University, Quezon City 1101,
14 Philippines

15 ⁴Department of Chemical and Environmental Engineering, University of Arizona, Tucson, AZ, USA

16 ⁵Philippine Nuclear Research Institute, Commonwealth Avenue, Diliman, Quezon City 1101, Philippines

17 ⁶Department of Hydrology and Atmospheric Sciences, University of Arizona, Tucson, AZ, USA

18

19 *Correspondence to:* Melliza Templonuevo Cruz (liz@observatory.ph)

20



21 Abstract

22 This paper presents novel results from size-resolved particulate matter (PM) mass, composition,
23 and morphology measurements conducted during the 2018 Southwest Monsoon (SWM) season in
24 Metro Manila, Philippines. Micro-Orifice Uniform Deposit Impactors (MOUDIs) were used to
25 collect PM sample sets that were analyzed for mass, morphology, black carbon (BC), and
26 composition of the water-soluble fraction. The bulk of the PM mass was between 0.18–1.0 μm
27 with a dominant mode between 0.32–0.56 μm . Similarly, most of the black carbon (BC) mass was
28 found between 0.10–1.0 μm (the so-called Greenfield gap), peaking between 0.18–0.32 μm , where
29 wet scavenging by rain is inefficient. In the range of 0.10 – 0.18 μm , BC constituted 78.1% of the
30 measured mass. Comparable contributions of BC (26.9%) and the water-soluble fraction (31.3%)
31 to total PM were observed and most of the unresolved mass, which in total amounted to 41.8%,
32 was for diameters exceeding 0.32 μm . The water-soluble ions and elements exhibited an average
33 combined concentration of 8.53 $\mu\text{g m}^{-3}$, with SO_4^{2-} , NH_4^+ , NO_3^- , Na^+ , and Cl^- as the major
34 contributors. Positive Matrix Factorization (PMF) was applied to identify the possible aerosol
35 sources and estimate their contribution to the water-soluble fraction of collected PM. The factor
36 with the highest contribution was attributed to “Aged/Transported” aerosol (48.0%) while “Sea
37 Salt” (22.5%) and “Combustion” emissions (18.7%) had comparable contributions.
38 “Vehicular/Resuspended Dust” (5.6%) as well as “Waste Processing” emissions (5.1%) were also
39 identified. Microscopy analysis highlighted the ubiquity of non-spherical particles regardless of
40 size, which is significant when considering calculations of parameters such as single scattering
41 albedo, asymmetry parameter, and extinction efficiency.

42 Results of this work have implications for aerosol impacts on public health, visibility, and regional
43 climate as each of these depend on physicochemical properties of particles as a function of size.
44 The significant influence from Aged/Transported aerosol to Metro Manila during the SWM season
45 indicates that local sources in this megacity do not fully govern this coastal area’s aerosol
46 properties and that PM in Southeast Asia can travel long distances regardless of the significant
47 precipitation and potential wet scavenging that could occur. That the majority of the regional
48 aerosol mass burden is accounted for by BC and other insoluble components has important
49 downstream effects on the aerosol hygroscopic properties, which depend on composition. The
50 results are relevant for understanding the impacts of monsoonal features on size-resolved aerosol
51 properties, notably aqueous processing and wet scavenging. Finally, the results of this work



52 provide contextual data for future sampling campaigns in Southeast Asia such as the airborne
53 component of the Cloud, Aerosol, and Monsoon Processes Philippines Experiment (CAMP²Ex)
54 planned for the SWM season in 2019. Aerosol characterization via remote-sensing is notoriously
55 difficult in Southeast Asia, which elevates the importance of datasets such as the one presented
56 here.
57



58 1. Introduction

59

60

61 Ambient atmospheric aerosol particles impact human health, visibility, climate, and the
62 hydrological cycle. Major factors governing these behaviors, such as deposition fraction in the
63 respiratory system and activation into cloud condensation nuclei (CCN), include size and chemical
64 composition. Therefore, size-resolved measurements of ambient aerosol particles can lend
65 additional insights to the behaviors and implications of particulate matter (PM) in the atmosphere.
66 One region of interest for characterization of aerosols is Southeast Asia due to increasing
67 urbanization and the exposure of the population to a variety of aerosol sources, both natural and
68 anthropogenic (Hopke et al., 2008). However, use of space-borne remote-sensing instrumentation
69 presents a challenge for characterization of aerosol in this region, due to issues such as varying
70 terrain and cloud cover (Reid et al., 2013).

70

71

72

73

74

75

76

77

78

79

80

81

82

83

84

85

86

87

88

89

The Philippines represents a country in Southeast Asia with a developing economy, rapid urbanization, old vehicular technology, and less stringent air quality regulations (e.g., Alas et al., 2017). It is also highly sensitive to the effects of climate change including prolonged dry periods and reductions in southwest monsoon (SWM) rainfall in recent decades (e.g., Cruz et al., 2013). Metro Manila is the country's capital and center of political and economic activities. Also referred to as the National Capital Region, Metro Manila is composed of 16 cities and a municipality that collectively occupy a land area of ~619 km². As of 2015, Metro Manila had a population of approximately 12.88 million (Philippine Statistics Authority, 2015). Of the cities comprising the Metro Manila area, the one that is the focus of this study, Quezon City, is the most populated (2.94 million people) with a population density of ~17,000 km⁻² as of 2015 (Philippine Statistics Authority, 2015).

The rainfall pattern in Southeast Asia is governed by topographic effects and the prevailing surface winds brought by the monsoons. Mountain ranges in the Philippines are generally oriented north to south in the eastern and western coasts. As such, northeasterly winds during the East Asian winter monsoon that starts in November brings wetness (dryness) on the eastern (western) coasts of the country. In contrast, the rainy season starts in May when the Western North Pacific subtropical high moves northeast and the Asian summer monsoon enables the propagation of southwesterly wind through the Philippines (Villafuerte et al., 2014). Metro Manila, located on the western side of the Philippines, therefore experiences wet (May-October) and dry (November-April) seasons. The large seasonal shift in prevailing wind directions can cause changes in the



90 source locations of aerosol transported to the Philippines and the subsequent direction in which
91 emissions from the Philippines are transported, such as to the northwest (e.g., Chuang et al., 2013)
92 or southwest (e.g., Farren et al., 2019). However, one interesting feature of Metro Manila is the
93 consistency of $PM_{2.5}/PM_{10}$ mass concentrations during both the dry (44/54 $\mu\text{g m}^{-3}$) and wet seasons
94 (43/55 $\mu\text{g m}^{-3}$) (Kim Oanh et al., 2006), which stands in contrast to typical assumptions that
95 increased wet scavenging during rainy seasons would lead to decreases in measured PM (e.g., Liao
96 et al., 2006). While similar results are observed in Chennai, India, this behavior is different than
97 other cities in Asia, including Bandung City (Indonesia), Bangkok (Thailand), Beijing (China),
98 and Hanoi City (Vietnam), that exhibit reduced $PM_{2.5}$ levels during the wet season as compared to
99 the dry season (Kim Oanh et al., 2006). While the total PM levels may stay constant across the wet
100 and dry seasons, seasonally-resolved analyses will provide additional insights into how the
101 composition, morphology, and sources (transported vs. local emissions) change on a seasonal
102 basis.

103 Metro Manila has been drawing growing interest for PM research owing to the significant
104 levels of black carbon (BC). A large fraction of PM in Metro Manila can be attributed to BC (e.g.,
105 ~50% of $PM_{2.5}$; Kim Oanh et al., 2006), with previously measured average values of BC at MO
106 reaching ~10 $\mu\text{g m}^{-3}$ for $PM_{2.5}$ (Simpas et al., 2014). The impacts of the high levels of BC present
107 on human health have also received attention (Kecorius et al., 2019). Identified major sources of
108 BC include vehicular, industrial, and cooking emissions (Bautista et al., 2014; Kecorius et al.,
109 2017). Vehicular emissions, especially along roadways where personal cars and motorcycles,
110 commercial trucks, and motorized public transportation, including powered tricycles and *jeepneys*,
111 are plentiful. For instance, measurements of $PM_{2.5}$ at the National Printing Office (NPO) located
112 alongside the major thoroughfare Epifanio de los Santos Avenue (EDSA) were on average 72 μg
113 m^{-3} ; this value is twice the average concentration at the Manila Observatory (MO), an urban mixed
114 site located approximately 5 km from NPO (Simpas et al., 2014). In addition to local emissions,
115 long-range transport of pollution, such as biomass burning, can also impact the study region (e.g.,
116 Xian et al., 2013; Reid et al., 2016a/b). However, most past work referenced above has focused on
117 either total $PM_{2.5}$ or PM_{10} composition, and therefore, detailed size-resolved composition
118 information has been lacking in this region. Like other monsoonal regions (Crosbie et al., 2015;
119 Qu et al., 2015), it is of interest for instance to know if products of aqueous processing (e.g., sulfate,
120 organic acids) during the monsoonal period, promoted by the high humidity, become more



121 prominent in certain size ranges to ultimately enhance hygroscopicity, which is otherwise
122 suppressed with higher BC influence.

123 A year-long sampling campaign (Cloud, Aerosol, and Monsoon Processes Philippines
124 Experiment (CAMP²Ex) weatHER and CompoSition Monitoring (CHECSM) study) was
125 established in July 2018 to collect size-resolved aerosol measurements in Metro Manila. The aim
126 of this study is to report size-resolved PM measurements taken over the course of the SWM (July-
127 October) of 2018 in Quezon City, Metro Manila, Philippines as part of CHECSM. The results of
128 this study are important for the following reasons: (i) they provide size-resolved analysis of BC in
129 an area previously characterized as having one of the highest BC mass percentages in the whole
130 world; (ii) they provide a basis for better understanding the unusual phenomenon of having similar
131 PM levels during a wet and dry season; (iii) they provide contextual data for contrasting with both
132 other coastal megacities and also other monsoonal regions; and (iv) they can lend insights into the
133 characteristics of aerosol transported both into and out of Metro Manila and how important local
134 sources are in Metro Manila relative to transported pollution. Outcomes of this study include (i)
135 the first size-resolved characterization of both aerosol composition and morphology in Metro
136 Manila for the SWM, with implications in terms of PM effects on climate, visibility, the
137 hydrological cycle, and public health owing to the dependence of these impacts on particle size;
138 (ii) archival data that contributes to the timeline of aerosol research in Metro Manila, and more
139 broadly Southeast Asia, where there is considerable concern over air pollution; and (iii) baseline
140 data for aerosol composition to be used to inform and assist research to be conducted during future
141 field campaigns in Southeast Asia including the same seasonal period (i.e., SWM) in 2019 as part
142 of CAMP²Ex, which will involve both surface and airborne measurements.

143 **2. Experimental Methods**

144 **2.1 Sample Site**

145 Sampling was performed at MO in Quezon City, Philippines (14.64° N, 121.08° E). The
146 sampling instrumentation was located on the 3rd floor of the MO office building (~85 m above
147 sea level). Figure 1 visually shows the sampling location and potential surrounding sources. Past
148 work focused on PM_{2.5} suggested that the study location is impacted locally mostly by traffic,
149 various forms of industrial activity, meat cooking from local eateries, and, based on the season,
150 biomass burning (Cohen et al., 2009). Fourteen sample sets were collected during the SWM season



151 (July-October 2018), with details about the operational and meteorological conditions during each
152 sample set shown in Table 1. Meteorological data were collected using a Davis Vantage Pro 2 Plus
153 weather station co-located with the aerosol measurements at MO. Except for precipitation, which
154 is reported here as accumulated rainfall, reported values for each meteorological parameter
155 represent averages for the sampling duration of each aerosol measurement.

156 The mean temperature during the periods of MOUDI sample collection ranged from 24.9
157 to 28.1° C, with accumulated rainfall ranging widely from no rain to up to 78.4 mm. To identify
158 sources impacting PM via long-range transport to the Metro Manila region, Figure 1a summarizes
159 the five-day back-trajectories for air masses arriving at MO on the days when samples were being
160 collected, calculated using the NOAA Hybrid Single-Particle Lagrangian Integrated Trajectory
161 (HYSPLIT) model (Stein et al., 2015; Rolph, 2016). Trajectory calculations were started at 00,
162 06, 12, and 18 hours in MO at the height of the MOUDI inlet using meteorological files from the
163 NCEP/NCAR Reanalysis dataset. Trajectory cluster analysis was conducted using TrajStat (Wang
164 et al., 2009). The back-trajectories in Figure 1a show that indeed 66% of the wind came from the
165 southwest during the sampling periods.

166 **2.2 MOUDI Sample Sets**

167 Particulate matter was collected on Teflon substrates (PTFE membrane, 2 µm pore, 46.2
168 mm, Whatman) in Micro-Orifice Uniform Deposit Impactors (MOUDI, MSP Corporation, Marple
169 et al., 2014). Size-resolved measurements were taken at the following aerodynamic cutpoint
170 diameters (D_p): 18, 10, 5.6, 3.2, 1.8, 1.0, 0.56, 0.32, 0.18, 0.10, 0.056 µm. For a subset of the
171 sampling periods, two pairs of MOUDI sets were collected simultaneously such that both sets in
172 each pair could undergo different types of analyses. One set in each pair underwent gravimetric
173 analysis using a Sartorius ME5-F microbalance. MOUDI set 13 was additionally examined with a
174 Multi-wavelength Absorption Black Carbon Instrument (MABI; Australian Nuclear Science and
175 Technology Organisation). This optically-based instrument quantifies absorption and mass
176 concentrations at seven wavelengths between 405 and 1050 nm; however, results are reported only
177 for 870 nm to be consistent with other studies as BC is the predominant absorber at that wavelength
178 (e.g., Ramachandran and Rajesh, 2007; Ran et al., 2016). One additional sample set for microscopy
179 analysis was collected for one hour on August 1 using aluminum substrates.

180 **2.3 Chemical Composition Analysis**



181 In order to preserve samples for additional analysis, each Teflon substrate was cut in half.
182 A half of each substrate was extracted in 8 mL of Milli-Q water (18.2 MΩ-cm) through sonication
183 for 30 min in a sealed polypropylene vial. A blank substrate was processed in the same method to
184 serve as a background control sample. Subsequent chemical analysis of the water-soluble
185 components in the aqueous extracts were performed using ion chromatography (IC; Thermo
186 Scientific Dionex ICS - 2100 system) for the following species: cations = Na⁺, NH₄⁺, Mg²⁺, Ca²⁺,
187 dimethylamine (DMA), trimethylamine (TMA), diethylamine (DEA); anions =, methanesulfonate
188 (MSA), pyruvate, adipate, succinate, maleate, oxalate, phthalate, Cl⁻, NO₃⁻, SO₄²⁻. Owing to co-
189 elution of TMA and DEA in the IC system, a cumulative sum of the two is reported here, which
190 represents an underestimate of their total mass concentration owing to overlap in parts of their
191 peaks. Limits of detection (LOD) were calculated for each species based on their respective
192 calibration curve (Table S1), with LOD being three times the standard deviation of the residuals
193 (predicted signal minus measured signal) divided by the slope of the calibration curve (Miller and
194 Miller, 2018).

195 The aqueous extracts were simultaneously characterized for elemental composition using
196 triple quadrupole inductively coupled plasma mass spectrometry (ICP-QQQ; Agilent 8800 Series)
197 for the following species: K, Al, Fe, Mn, Ti, Ba, Zn, Cu, V, Ni, P, Cr, Co, As, Se, Rb, Sr, Y, Zr,
198 Nb, Mo, Ag, Cd, Sn, Cs, Hf, Tl, Pb. Limits of detection of the examined elements were calculated
199 automatically by the ICP-QQQ instrument and were in the ppt range (Table S1). The sample
200 concentrations represent an average of three separate measurements with a standard deviation of
201 3% or less.

202 Note that some species were detected by both IC and ICP-QQQ (i.e., Na⁺, K⁺, Mg²⁺, Ca²⁺),
203 and that the IC concentrations are used here for all repeated species with the exception of K⁺ owing
204 to better data quality from ICP-QQQ. All IC and ICP-QQQ species concentrations for samples
205 have been corrected by subtracting concentrations from background control samples.

206 **2.4 Microscopy Analysis**

207 As already noted, one MOUDI set on August 1 was devoted to microscopy analysis.
208 Morphology and additional elemental composition analysis was carried out on this set of aluminum
209 substrates using scanning electron microscopy equipped with energy dispersive X-ray
210 spectroscopy (SEM-EDX) in the Kuiper Imaging cores at the University of Arizona. Secondary



211 electron (SE) imaging and EDX elemental analysis were performed using a Hitachi S-4800 high
212 resolution SEM coupled to a Noran system Six X-ray Microanalysis System by Thermo Fisher
213 Scientific. EDX analysis on individual particles was performed with 30 kV accelerating voltage to
214 obtain weight percentages of individual elements. SEM-EDX results showed that the background
215 control aluminum substrate was dominated by Al (88.27%), with minor contributions from Ag
216 (5.34%), C (4.87%), O (0.79%), Fe (0.67%), and Co (0.05%). Such contributions were manually
217 subtracted from spectra of individual particles on sample substrates, with the remaining elements
218 scaled up to hundred percent. Image processing was conducted with Image J software to measure
219 particle dimensions and adjust the contrast and brightness of images to provide better visualization.

220 **2.5 Computational Analysis**

221 This study reports basic descriptive statistics for chemical concentrations and correlations
222 between different variables. Statistical significance hereafter corresponds to 95% significance
223 based on a two-tailed Student's t-test. To complement correlative analysis for identifying sources
224 of species, positive matrix factorization (PMF) modeling was carried out using the United States
225 Environmental Protection Agency's (US EPA) PMF version 5. Species considered as "strong"
226 based on high signal-to-noise ratios ($S/N > 1$) and those with at least 50% of the concentrations
227 above the detection limit were used in the PMF modeling (Norris et al., 2014). Data points with
228 concentrations exceeding the LOD had uncertainty quantified as follows:

229

$$230 \quad \sigma_{ij} = 0.05 \cdot X_{ij} + LOD_{ij} \quad (\text{Equation 1})$$

231

232 where σ_{ij} , X_{ij} , and LOD_{ij} are the uncertainty, concentration, and LOD, respectively, of the j^{th}
233 species in the i^{th} sample (Reff et al., 2007). When concentration data were not available for a
234 particular stage of a MOUDI set for a species, the geometric mean of the concentrations for that
235 MOUDI stage and species was applied with uncertainty counted as four times the geometric mean
236 value (Polissar et al., 1998; Huang et al., 1999). A 25% extra modeling uncertainty was applied
237 to account for other sources of errors such as changes in the source profiles and chemical
238 transformations (Dumanoglu et al., 2014; Norris et al., 2014). The model was run 20 times with a
239 randomly chosen starting point for each run.

240 **3. Results**



241 3.1 Total Mass Concentrations and Charge Balance

242 The average total mass concentration (\pm standard deviation) of water-soluble species across
243 all MOUDI stages (Table 1) during the study period was $8.53 \pm 4.48 \mu\text{g m}^{-3}$ (range = 2.7–16.6 μg
244 m^{-3}). The species contributing the most to the total water-soluble mass concentration during the
245 SWM included SO_4^{2-} ($44\% \pm 6\%$), NH_4^+ ($18\% \pm 5\%$), NO_3^- ($10 \pm 3\%$), Na^+ ($8 \pm 3\%$), and Cl^- (6%
246 $\pm 3\%$). The meteorological parameters from Table 1 best correlated to total water-soluble mass
247 concentrations were temperature ($r = 0.64$) and rainfall ($r = -0.49$). The highest total mass
248 concentration (set MO13/14 = $16.6 \mu\text{g m}^{-3}$) occurred during the period with one of the highest
249 average temperatures (27.8°C) and second least total rainfall (0.8 mm). Other sampling periods
250 with high mass concentrations (sets MO7, MO8, and MO12) coincided with the highest
251 temperature and lowest rainfall observations. High temperatures, and thus more incident solar
252 radiation, presumably enhanced production of secondary aerosol species via photochemical
253 reactions as has also been observed in other regions for their respective monsoon season (Youn et
254 al., 2013). Low rainfall is thought to have been coincident with reduced wet scavenging of aerosol
255 at the study site as has been demonstrated for other regions such as North America (Tai et al.,
256 2010) and megacities such as Tehran (Crosbie et al., 2014). However, set MO11 exhibited a very
257 low concentration even with high temperature and lack of rainfall, which may be due to changes
258 in the source and transport of aerosol since this sample set coincided with a significant change in
259 average wind direction (290.2° for MO11 vs. $90.1^\circ - 127.5^\circ$ for all other MOUDI sets). While the
260 reported rainfall measurements were taken at MO, inhomogeneous rainfall patterns in the regions
261 surrounding the Philippines could also contribute to the wet scavenging of PM, thereby lowering
262 the quantity of transported particles reaching the sample site. Future work will address the
263 influence of spatiotemporal patterns of precipitation on PM loadings in the Philippines as a point
264 measurement at an aerosol observing site may be misleading.

265 On two occasions, two simultaneous MOUDI sets (Sets MO3/MO4 and MO13/MO14)
266 were collected for the potential to compare different properties that require separate substrates.
267 The total mass concentrations based on gravimetric analysis of sets MO3 and MO13 were $18.6 \mu\text{g}$
268 m^{-3} and $53.0 \mu\text{g m}^{-3}$, respectively (Figure 2). Both sets exhibited a dominant concentration mode
269 between $0.32\text{--}0.56 \mu\text{m}$ and the MO3 set was different in that it exhibited bimodal behavior with a
270 second peak between $1.8\text{--}3.2 \mu\text{m}$. The sum of speciated water-soluble species accounted for only
271 27.8% and 31.3% of the total gravimetric mass of sets MO3 and MO13, respectively, indicative



272 of significant amounts of water-insoluble species undetected by IC and ICP-QQQ. When adding
273 the total mass of BC ($14.3 \mu\text{g m}^{-3}$) to the other resolved species from set MO13 (the one time BC
274 was measured), there was still $22.1 \mu\text{g m}^{-3}$ of unresolved mass (41.8% of total PM). Most of the
275 unaccounted mass was for $D_p > 0.32 \mu\text{m}$. The observation of BC accounting for 26.9% of total PM
276 ($14.3 \mu\text{g m}^{-3}$) is consistent with past work highlighting the significant fraction of BC in the ambient
277 aerosol of Manila (Kim Oanh et al., 2006; Bautista et al., 2014; Simpas et al., 2014; Kecorius et
278 al., 2017). However, this fraction of BC is very high compared to measurements during the
279 monsoon season in other parts of the world. The mass fraction of BC in total suspended PM
280 (TSPM) was 1.6%/2.2% for the monsoon season in 2013/2014 in Kadapa in southern India, even
281 though the TSPM measured was comparable to that in Manila (64.9 and $49.9 \mu\text{g m}^{-3}$, for 2013 and
282 2014 in Kadapa, respectively) (Begam et al., 2017). Multiple studies during the monsoon season
283 in a coastal region in southwest India showed BC mass contributions of 1.9 – 5% (Aswini et al.,
284 2019 and references therein). Airborne measurements around North America and in Asian outflow
285 revealed that BC accounted for only ~1-2% of $\text{PM}_{1.0}$ (Shingler et al., 2016) and ~5-15% of
286 accumulation mode aerosol mass (Clarke et al., 2004), respectively.

287 To investigate further about the missing species, a charge balance was carried out for all
288 MOUDI sets (Table 2) to compare the sum of charges for cations versus anions based on IC
289 analysis including K from ICP-QQQ analysis (species listed in Section 2.3). The slope of the
290 charge balances (cations on y-axis) for the cumulative dataset was 1.33 and ranged from 0.89 to
291 1.41 for the 12 individual MOUDI sets that had IC and ICP-QQQ analysis conducted on them.
292 Eleven of the 12 sets exhibited slopes above unity indicating that there was a deficit in the amount
293 of anions detected, which presumably included species such as carbonate and various organics. To
294 further determine if there were especially large anion or cation deficits in specific size ranges,
295 slopes are also reported for $0.056\text{--}1 \mu\text{m}$ and $> 1 \mu\text{m}$. There were no obvious differences other than
296 two MOUDI sets exhibited slopes below 1.0 for the smaller diameter range ($0.056\text{--}1 \mu\text{m}$) while
297 all slopes exceeded unity for $> 1 \mu\text{m}$.

298 3.2 Mass Size Distributions and Morphology

299 3.2.1 Black Carbon

300 The size-resolved nature of BC has not been characterized in Manila and MOUDI set
301 MO13 offered a view into its mass size distribution (Figure 3a). There was a pronounced peak



302 between 0.18–0.32 μm ($5.0 \mu\text{g m}^{-3}$), which is evident visually in the substrate's color when
303 compared to all other stages of that MOUDI set (Figure 3b). This observed peak in the mass size
304 distribution of BC is similar to previous studies of the outflow of East Asian countries (Shiraiwa
305 et al., 2008), biomass burning and urban emissions in Texas (Schwarz et al., 2008), measurements
306 in the Finnish Arctic (Raatikainen et al., 2015), and airborne measurements over Europe
307 (Reddington et al., 2013). In contrast, measurements in Uji, Japan showed a bimodal size
308 distribution for the mass concentration of BC in the submicrometer range (Hitzenberger and
309 Tohno, 2001). In the present study, there were significant amounts of BC extending to as low as
310 the 0.056–0.1 μm MOUDI stage ($0.28 \mu\text{g m}^{-3}$) and extending up in the supermicrometer range with
311 up to $0.25 \mu\text{g m}^{-3}$ measured between 1.8–3.2 μm . Remarkably, BC accounted for approximately
312 78.1% (51.8%) by mass of the total PM in the range of 0.10 – 0.18 μm (0.18 – 0.32 μm). For
313 comparison, the mass percent contribution of BC measured in the megacity of Nanjing, China was
314 3.3% (1.6%) at 0.12 (0.08) μm (Ma et al., 2017). Based on visual inspection of color on all
315 MOUDI sets, MO13 appears to be representative of the other sets based on the relative intensity
316 of the color black on substrates with different cutpoint diameters (Figure 3b); the 0.18–0.32 μm
317 substrate always was the most black, with varying degrees of blackness extending consistently into
318 the supermicrometer stages.

319 Microscopy analysis revealed evidence of non-spherical particles in each MOUDI stage
320 below 1 μm (Figure 4), which is significant as the common assumption theoretically is that
321 submicrometer particles are typically spherical (e.g., Mielonen et al., 2011). Errors in this
322 assumption impact numerical modeling results and interpretation of remote sensing data for
323 aerosols (e.g., Kahnert et al., 2005) owing to incorrect calculations of parameters such as single
324 scattering albedo, asymmetry parameter, and extinction efficiency (e.g., Mishra et al., 2015). Some
325 studies have noted that submicrometer particles could be composed of an agglomeration of small
326 spherical particles originally formed through gas-to-particle conversion processes (Almeida et al.,
327 2019), which could potentially explain the appearance for some of the observed particles in Figure
328 4. Since only single particles were examined that may not be fully representative of all particles
329 on a particular MOUDI substrate, it is noteworthy that all five particles shown between 0.056 – 1
330 μm were irregularly shaped with signs of both multi-layering and constituents adhered to one
331 another. The images show that a potentially important source of BC in the area could be soot
332 aggregates, which are formed by a vaporization-condensation process during combustion often



333 associated with vehicular exhaust (e.g., Chen et al., 2006; Chithra and Nagendra, 2013; Wu et al.,
334 2017). Kecorius et al. (2017) projected that 94% of total roadside refractory PM in the same study
335 region was linked to *jeepneys*, with number concentration modes at 20 and 80 nm. They associated
336 the larger mode with soot agglomerates, which is consistent with the smallest MOUDI size range
337 examined here (0.056–0.1 μm ; Figure 4b) exhibiting signs of agglomeration.

338 The total BC mass concentration integrated across all stages of MOUDI set MO13 (14.3
339 $\mu\text{g m}^{-3}$) was remarkably high in contrast to BC levels measured via either filters, aethalometers, or
340 single particle soot photometers in most other urban regions of the world (Metcalf et al., 2012 and
341 references therein): Los Angeles Basin (airborne: 0.002–0.53 $\mu\text{g m}^{-3}$), Atlanta, Georgia (ground:
342 0.5–3.0 $\mu\text{g m}^{-3}$), Mexico City (airborne: 0.276–1.1 $\mu\text{g m}^{-3}$), Sapporo, Japan (ground: 2.3–8.0 $\mu\text{g m}^{-3}$),
343 Beijing, China (ground: 6.3–11.1 $\mu\text{g m}^{-3}$), Bangalor, India (ground: 0.4–10.2 $\mu\text{g m}^{-3}$), Paris,
344 France (ground: 7.9 $\mu\text{g m}^{-3}$), Dushanbe, Russia (ground: 4–20 $\mu\text{g m}^{-3}$), Po Valley, Italy (ground:
345 0.5–1.5 $\mu\text{g m}^{-3}$), Thessaloniki, Greece (ground: 3.3–8.9 $\mu\text{g m}^{-3}$). This is intriguing in light of
346 extensive precipitation, and thus wet scavenging of PM, during the study period, which is offset
347 by enormous anthropogenic emissions in the region such as by powered vehicles like the *jeepneys*
348 that are notorious for BC exhaust (Kecorius et al., 2017).

349 A possible explanation for the large contribution of BC to PM, and the persistence of PM
350 after rain events (Kim Oanh et al., 2006), is that the BC is not efficiently scavenged by precipitating
351 rain drops. Small particles enter rain drops via diffusion whereas large particles enter via
352 impaction. However, particles with a diameter in the range of 0.1–1 μm (known as the Greenfield
353 gap) are too large to diffuse efficiently and too small to impact, and are therefore not efficiently
354 scavenged (Seinfeld and Pandis, 2016). Absorption spectroscopy of set MO13 (Figure 2b) reveals
355 that 95% of the BC mass is concentrated in the Greenfield gap, and thus the removal of BC due to
356 precipitation is inefficient. The Greenfield gap contains $62 \pm 11\%$ of the total mass (calculated for
357 MO3/MO13) and $65 \pm 10\%$ of the water-soluble mass (calculated for the other 12 MO sets).

358 3.2.2 Water-Soluble Ions

359 There were two characteristic mass size distribution profiles for the water-soluble ions
360 speciated by IC depending on whether the species were secondarily produced via gas-to-particle
361 conversion or associated with primarily emitted supermicrometer particles. The average IC species
362 mass concentration profile across all MOUDI sets is shown in Figure 5. Secondarily produced



363 species exhibited a mass concentration mode between 0.32–0.56 μm , including common inorganic
364 species (SO_4^{2-} , NH_4^+), MSA, amines (DMA, TMA+DEA), and a suite of organic acids, such as
365 oxalate, phthalate, succinate, and adipate, produced via precursor volatile organic compounds
366 (VOCs). Two organic acids with peaks in other size ranges included maleate (0.56–1 μm) and
367 pyruvate (0.1–0.18 μm). Sources of the inorganics are well documented with SO_4^{2-} and NH_4^+
368 produced by precursor vapors SO_2 and NH_3 , respectively, with ocean-emitted dimethylsulfide
369 (DMS) as an additional precursor to SO_4^{2-} and the primary precursor to MSA.

370 Precursors leading to secondarily produced alkyl amines such as DMA, TMA, and DEA
371 likely originated from a combination of industrial activity, marine emissions, biomass burning,
372 vehicular activity, sewage treatment, waste incineration, and the food industry (e.g., Facchini et
373 al., 2008; Sorooshian et al., 2009; Ge et al., 2011; VandenBoer et al., 2011); another key source of
374 these species, animal husbandry (Mosier et al., 1973; Schade and Crutzen, 1995; Sorooshian et al.,
375 2008), was ruled out owing to a scarcity of such activity in the study region. Secondarily produced
376 amine salts likely were formed with SO_4^{2-} as the chief anion owing to its much higher
377 concentrations relative to NO_3^- or organic acids. Dimethylamine was the most abundant amine
378 similar to other marine (Muller et al., 2009) and urban regions (Youn et al., 2015); the average
379 concentration of DMA integrated over all MOUDI stages for all sample sets was 62.2 ng m^{-3} in
380 contrast to 29.8 ng m^{-3} for TMA+DEA. For reference, the other key cation (NH_4^+) participating in
381 salt formation with acids such as H_2SO_4 and HNO_3 was expectedly much more abundant (1.64 μg
382 m^{-3}). With regard to the competitive uptake of DMA versus NH_3 in particles, the molar ratio of
383 DMA: NH_4^+ exhibited a unimodal profile between 0.1–1.8 μm with a peak of 0.022 between 0.32–
384 0.56 μm and the lowest values at the tails (0.004 between 0.1–0.18 and 1–1.8 μm); DMA was not
385 above detection limits for either $D_p < 0.1 \mu\text{m}$ or $D_p > 1.8 \mu\text{m}$. The molar ratios observed were
386 consistent with values measured in urban air of Tucson, Arizona and coastal air in Marina,
387 California (0–0.04; Youn et al., 2015) and near the lower end of the range measured in rural and
388 urban air masses sampled near Toronto (0.005–0.2; VandenBoer et al., 2011).

389 The most abundant organic acid was oxalate ($195 \pm 144 \text{ ng m}^{-3}$), followed by succinate (21
390 $\pm 41 \text{ ng m}^{-3}$), phthalate ($19 \pm 25 \text{ ng m}^{-3}$), maleate ($17 \pm 15 \text{ ng m}^{-3}$), and adipate ($5 \pm 8 \text{ ng m}^{-3}$). The
391 observation of mass concentrations increasing with decreasing carbon number for dicarboxylic
392 acids (i.e., oxalate > succinate > adipate) is consistent with many past studies for other regions as
393 larger chain acids undergo oxidative decay to eventually form oxalate (e.g., Kawamura and



394 Ikushima, 1993; Kawamura and Sakaguchi, 1999; Sorooshian et al., 2007). Maleate is an
395 unsaturated dicarboxylic acid emitted from gas and diesel engines (Rogge et al., 1993) and a
396 product from the photo-oxidation of benzene (Kawamura and Ikushima, 1993). The aromatic
397 dicarboxylic acid phthalate is a known photo-oxidation product of naphthalene and stems largely
398 from plastic processing and fuel combustion (Fraser et al., 2003; Kautzman et al., 2010; Fu et al.,
399 2012; Kleindienst et al., 2012). The oxidation product (MSA) of ocean-derived DMS exhibited an
400 overall average concentration of $11 \pm 7 \text{ ng m}^{-3}$, which is near the lower end of the range of levels
401 reported in other coastal and marine environments (from undetected up to $\sim 200 \text{ ng m}^{-3}$) (e.g.,
402 Saltzman et al., 1983, 1986; Berresheim 1987; Watts et al., 1987; Burgermeister and Georgii,
403 1991; Sorooshian et al., 2015; Xu and Gao, 2015).

404 Water-soluble species exhibiting a peak in the supermicrometer range, usually between
405 $1.8\text{--}5.6 \mu\text{m}$, include those with known affiliations with sea salt (Na^+ , Cl^- , K^+ , Mg^{2+}) and crustal
406 materials such as dust (Ca^{2+}). Nitrate peaked between $1.8\text{--}3.2 \mu\text{m}$, and was best correlated with
407 Na^+ and Mg^{2+} , suggestive of HNO_3 partitioning to sea salt as has been observed in other coastal
408 regions (e.g., Prabhakar et al., 2014a). There was very little NO_3^- in the submicrometer range (0.05
409 $\pm 0.04 \mu\text{g m}^{-3}$) in contrast to supermicrometer sizes ($0.78 \pm 0.47 \mu\text{g m}^{-3}$). More submicrometer
410 NO_3^- in the form of NH_4NO_3 would be expected if there was an excess of NH_3 after neutralizing
411 SO_4^{2-} . The mean ammonium-to-sulfate molar ratio for submicrometer sizes was 2.32 ± 0.52 (range:
412 $1.11 - 2.78$), with full neutralization of SO_4^{2-} in 10 of 12 MOUDI sets. Thus, there was a non-
413 negligible excess in NH_3 that presumably participated in salt formation with HNO_3 and organic
414 species. The significant levels of NO_3^- in the same mode as Na^+ and Cl^- contributed to the
415 significant Cl^- depletion observed, as the mean $\text{Cl}^-:\text{Na}^+$ mass ratio between $1\text{--}10 \mu\text{m}$ (i.e., range of
416 peak sea salt influence) was 0.81 ± 0.28 , which is much lower than the ratio for pure sea salt (1.81)
417 (Martens et al., 1973). The subject of Cl^- depletion in this region will be investigated more
418 thoroughly in subsequent work.

419 Figure 6 shows SEM images of representative single particles in each supermicrometer
420 stage. As would be expected for sea salt and crustal material, most of the particles shown are not
421 spherical. Interestingly, only the particle shown between $1\text{--}1.8 \mu\text{m}$ was close to being spherical.
422 Its composition based on EDX analysis was accounted for mostly by carbon (93.7%) with lower
423 amounts of oxygen (5.8%) and Fe (0.5%). Sea salt particles were found in the next two stages
424 owing to the highest combined weight percentages of Na^+ and Cl^- based on EDX analysis: $1.8\text{--}3.2$



425 $\mu\text{m} = 36.9\%$; $3.2\text{--}5.6 \mu\text{m} = 46.9\%$. The salt particles are not necessarily cubical but more rounded
426 with signs of agglomeration. These two particles were the only ones among the 11 MOUDI stages
427 exhibiting an EDX signal for S, with contributions amounting to $\sim 2\%$ in each particle. This may
428 be linked to natural SO_4^{2-} existing in sea salt particles. Also, the particle between $3.2\text{--}5.6 \mu\text{m}$
429 contained a trace amount of Sc (1%). The largest three particles ($\geq 5.6 \mu\text{m}$) were expectedly
430 irregularly shaped with both sharp and rounded edges, comprised mostly of oxygen, Al, Fe, and
431 Ca based on EDX analysis.

432 3.2.3 Water-Soluble Elements

433 Averaged data across all MOUDI sets reveal that ICP-QQQ elements exhibited a variety
434 of mass concentration profiles ranging from a distinct mode in either the sub- or supermicrometer
435 range to having multiple modes below and above $1 \mu\text{m}$ (averages across all MOUDI sets shown
436 in Figure 7). There were several elements with only one distinct peak, being in one of the two
437 stages between $0.18\text{--}1.0 \mu\text{m}$, including As, Cd, Co, Cr, Cs, Cu, Hf, Mn, Mo, Ni, Rb, Se, Sn, Tl, V,
438 Pb, and Zn. In contrast, the following elements exhibited only one distinct peak in the
439 supermicrometer range: Al, Ba, P, Sr, Ti, Y, and Zr. The rest of the elements exhibited more
440 complex behavior with two distinct peaks in the sub- and supermicrometer range (Ag, Fe, Nb).
441 The following section discusses relationships between all of the ions and elements with a view
442 towards identifying characteristic sources.

443 3.3 Characteristic Sources and Species Relationships

444 A combination of PMF and correlation analysis helped identify clusters of closely related
445 species stemming from distinct sources. The final PMF solution, based on five groups of species
446 (Figure 8), passed criteria associated with being physically valid and the close proximity of the
447 calculated ratio of $Q_{\text{true}}:Q_{\text{expected}}$ (1.2) to 1.0. There was a high coefficient of variation between
448 measured and predicted mass concentration when summing up all species for each MOUDI stage
449 ($r^2 = 0.79$; sample size, $n = 132$), which added confidence in relying on the PMF model for source
450 apportionment of PM. The five distinct clusters were named for their most plausible sources based
451 on the species included in the groupings, with their overall contributions to the total mass based
452 on PMF analysis shown in parenthesis (Table 3): Aged/Transported (48.0%), Sea Salt (22.5%),
453 Combustion (18.7%), Vehicular/Resuspended Dust (5.6%), and Waste Processing (5.1%). For



454 reference, a previous study near the northwestern edge of the Philippines identified six source
455 factors for PM_{2.5} that are fairly similar to those here (Bagtasa et al., 2018): sea salt, resuspended
456 fine dust, local solid waste burning, and long range transport of (i) industrial emissions, (ii) solid
457 waste burning, and (iii) secondary sulfate. Each of our five groupings will be discussed in detail
458 below in decreasing order of contribution to total measured mass concentrations.

459 3.3.1 Aged/Transported Aerosol

460 Although not due to one individual source, there was a distinct PMF factor that included
461 species commonly produced via gas-to-particle conversion processes (NH₄⁺, SO₄²⁻, MSA,
462 oxalate). Correlation analysis (Table 4) also pointed to a large cluster of species significantly
463 related to each other, including the aforementioned ions and a suite of other organic acids
464 (phthalate, succinate, adipate), MSA, and DMA. The latter three inorganic and organic acid ions
465 exhibited significant correlations with each other ($r \geq 0.68$), but also with several elements ($r \geq$
466 0.36: K, V, Rb, Cs, Sn), which were likely co-emitted with the precursor vapors of the secondarily
467 produced ions. Although BC concentrations were quantified from set MO13, their
468 interrelationships with water-soluble ions from simultaneously collected set MO14 are
469 representative for other sets. The results showed that BC was significantly correlated (r : 0.61-0.92)
470 with 15 species, including those mentioned above (owing to co-emission) and also a few elements
471 that were found via PMF to be stronger contributors to the Combustion source discussed in Section
472 3.3.3 (Ni, Cu, As, Se, Cd, Tl, Pb).

473 This PMF source factor is referred to as Aged/Transported owing to its characteristic species
474 being linked to sources distant from the sample site. Examples include MSA and DMA being
475 secondarily produced from ocean-derived gaseous emissions (e.g., Sorooshian et al., 2009), and K
476 stemming from biomass burning emissions from upwind regions such as Sumatra and Borneo
477 (Xian et al., 2013). Previous studies (Reid et al., 2012; Wang et al., 2013) have shown that
478 phenomena such as SWM and El-Nino events not only influence biomass burning activities in the
479 Malay Peninsula but also impact the transport and distribution of emissions in the study region.
480 For instance, Reid et al. (2016b) showed that enhancement in monsoonal flow facilitates the
481 advection of biomass burning and anthropogenic emissions to the Philippines from Sumatra and
482 Borneo. Subsequent work will investigate more deeply the impact of biomass burning from those
483 upwind regions on the sample site during the SWM.



484 While NH_4^+ and SO_4^{2-} require time for production owing to being secondarily produced
485 from precursor vapors (i.e., SO_2 , NH_3), oxalate is the smallest dicarboxylic acid and requires
486 lengthier chemistry pathways for its production and thus is more likely produced in instances of
487 aerosol transport and aging (e.g., Wonaschuetz et al., 2012; Ervens et al., 2018). The various
488 elements associated with this cluster are co-emitted with the precursors to the aforementioned ions
489 and are linked to a variety of sources: metallurgical processes (Anderson et al., 1988; Csavina et
490 al., 2011; Youn et al., 2016), fuel combustion (Nriagu, 1989; Allen et al., 2001; Shafer et al., 2012;
491 Rocha and Correa, 2018), residual oil combustion (Watson et al., 2004), biomass burning (Maudlin
492 et al., 2015), marine and terrestrial biogenic emissions (Sorooshian et al., 2015), and plastics
493 processing (Fraser et al., 2003). In addition, there is extensive ship traffic in the general study
494 region, which is a major source of species in this cluster of species, particularly V and SO_4^{2-} (e.g.,
495 Murphy et al., 2009; Coggon et al., 2012).

496 PMF analysis suggested that the Aged/Transported factor contributed 48.0% to the total
497 water-soluble mass budget during the study period. Most of the contribution resided in the
498 submicrometer range (68.9%) unlike the supermicrometer range (18.6%), which is consistent with
499 the overall mass size distribution of total PM peaking in the submicrometer range (Figure 2). The
500 reconstructed mass size distribution for this PMF source factor shows the dominance of the mass
501 in the submicrometer range with a peak between 0.32–0.56 μm (Figure 9). The correlation matrices
502 for the sub- and supermicrometer size ranges also show that the correlations between the species
503 most prominent in the Aged/Transported category are stronger for the former size range (Tables
504 S2-S3). The contribution of this PMF factor to the supermicrometer range is likely associated with
505 species secondarily produced on coarse aerosol such as dust and sea salt. This is evident in the
506 individual species mass size distributions where there is a dominant submicrometer mode but also
507 non-negligible mass above 1 μm .

508 Even though the PM in a heavily populated urban region, such as Metro Manila, is typically
509 thought to be dominated by local sources of aerosols, the current PMF results show that the largest
510 contributions to water-soluble aerosol mass are from Aged/Transported pollution. This finding is
511 contrary to the expectation that (a) the signal of transported aerosols would be lost in the noise of
512 locally-produced aerosols, and (b) the removal of aerosols over the ocean surrounding the
513 Philippines by processes such as wet scavenging would significantly reduce the contribution of
514 transported aerosols. Even though other cities may have different pollution signatures, varying in



515 pollutant type and amount, this phenomenon of Aged/Transported pollution forming a significant
516 portion of the water-soluble mass may be applicable to other cities, especially those in Southeast
517 Asia.

518 3.3.2 Sea Salt

519 As the MO sampling site is approximately 13 km from the nearest shoreline (Figure 1a)
520 and downwind of Manila Bay in the SWM season, there was a great potential for marine emissions
521 to impact the samples. There were several species with similar mass size distributions (mode: 1.8–
522 5.6 μm) and highly correlated total mass concentrations ($r \geq 0.51$) that are linked to sea salt: Cl,
523 Na⁺, Ca²⁺, Mg²⁺, Ba, and Sr. The correlations between these species were stronger when examining
524 just the supermicrometer range as compared to the submicrometer range (Tables S2-S3). The
525 majority of these species was used in PMF analysis and formed a distinct cluster amounting to
526 22.0% of the total study period's mass budget. This source contributed only 0.6% to the
527 submicrometer mass concentration but 53.5% for the supermicrometer size range. The
528 reconstructed mass size distribution for this source factor is shifted farthest to the larger diameters
529 as compared to the other four sources with a peak between 1.8-3.2 μm (Figure 9).

530 It is noteworthy that this factor has the highest share of NO₃⁻ among all identified sources.
531 This result is consistent with mass size distributions shown in Figure 5 in which NO₃⁻ peaks in the
532 supermicrometer range similar to sea salt constituents (e.g., Na⁺ and Cl⁻). Although sea salt
533 particles naturally contain NO₃⁻ (Seinfeld and Pandis, 2016) (mass ratio of NO₃⁻:Na⁺ = 9.8×10^{-8}
534 – 6.5×10^{-5}), the extremely high ratio of NO₃⁻:Na⁺ (mass ratio ~1.8) suggests that only a negligible
535 portion of NO₃⁻ in this factor originated from primary sea salt particles. Thus, the majority of NO₃⁻
536 is most likely due to HNO₃ partitioning to existing sea salt particles (e.g., Fitzgerald, 1991; Allen
537 et al., 1996; Dasgupta et al., 2007; Maudlin et al., 2015). In addition, the Cl⁻:Na⁺ mass ratio in this
538 profile (0.65) is smaller than that in sea salt particles (1.81), indicating high Cl⁻ depletion mainly
539 due to reactions of HNO₃ with NaCl (Ro et al., 2001; Yao et al., 2003; Braun et al., 2017).
540 Moreover, elevated loadings of trace elements (e.g., Ba, Cu, Zn, and Co) could be linked to mixing
541 of marine emissions with urban sources (e.g., vehicle and industrial emissions) during their
542 transport inland to the sampling site (Roth and Okada, 1998). This process of aging is consistent
543 with the observed morphology of the sea salt particles in this study, revealing non-cubical shapes
544 that are rounded owing to the likely addition of acidic species such as HNO₃ (Figure 6).



545 3.3.3 Combustion

546 There are numerous sources of combustion in the study region including a variety of mobile
547 sources (e.g., cars, utility vehicles, trucks, buses, motorcycles) and stationary sources (e.g., power
548 stations, cement works, oil refineries, boiler stations, utility boilers). Consequently, the next
549 highest contributor to total mass during the study period according to PMF (18.7%) was the cluster
550 of species including Ni, As, Co, P, Mo, and Cr, which is defined as the Combustion factor. These
551 species have been reported to be rich in particles emitted from combustion of fossil fuel and
552 residual oil (Linak and Miller, 2000; Allen et al., 2001; Wasson et al., 2005; Mahowald et al.,
553 2008; Mooibroek et al., 2011; Prabhakar et al., 2014b). Although not included in PMF analysis,
554 other species significantly correlated with the previous ones include maleate and Ag, which also
555 stem from fuel combustion (Kawamura and Kaplan, 1987; Lin et al., 2005; Sorooshian et al.,
556 2007). Ag specifically is an element in waste incinerator fly ash (Buchholz and Landsberger, 1993;
557 Tsakalou et al., 2018) and its strong correlation with Co ($r = 0.85$) and Mo ($r = 0.64$) provides
558 support for this source factor being linked to combustion processes. Maleate is commonly found
559 in engine exhaust (Kawamura and Kaplan, 1987), while Cr is a tracer for power plant emissions
560 (Singh et al., 2002; Behera et al., 2015). Of all species examined in this study, BC was best
561 correlated with As ($r = 0.92$), while its correlation with Ni ($r = 0.85$) was among the highest.

562 As the elements in this cluster peaked in concentration in the submicrometer mode, the
563 weight percentage of this factor is more than double below $1\ \mu\text{m}$ (23.9%) as compared to above $1\ \mu\text{m}$
564 (11.3%). The reconstructed mass size distribution for this source factor peaks between 0.18--
565 $0.32\ \mu\text{m}$, which is smaller than the modal diameter range for the Aged/Transported source factor
566 ($0.32\text{--}0.56\ \mu\text{m}$) likely owing to closer sources and thus less time for growth to occur via
567 condensation and coagulation.

568 3.3.4 Vehicular/Resuspended Dust

569 The next PMF source factor contains chemical signatures of dust because of high
570 contributions to Al, Ti, Ca, and Fe. These crustal elements are strongly related to resuspension of
571 dust by traffic and construction activities (Singh et al., 2002; Harrison et al., 2011). Other elements
572 that were prominent in this factor included Zr, Y, Mn, Cr, and Ba, which are associated with tire
573 and brake wear (Adachi and Tainosho, 2004; Gietl et al., 2010; Song and Gao, 2011; Harrison et
574 al., 2012; Vossler et al., 2016), although some of them can be linked to the exhaust as well (e.g.,



575 Lin et al., 2005; Song and Gao, 2011). This source is named Vehicular/Resuspended Dust and
576 contributed 5.6% to the total study period's mass concentrations.

577 The weight percentage contribution of this factor was much higher for the supermicrometer
578 range (11.3%) as compared to the submicrometer range (1.5%), which is consistent with the Sea
579 Salt source factor owing to similar mass size distributions of the individual species associated with
580 the two source categories (Figures 5 and 7). Additional species correlated significantly with the
581 crustal species included Hf and Nb, which also exhibited mass peaks between 1.8–3.2 μm . The
582 reconstructed mass size distribution for this source factor is similar to that of Sea Salt in that there
583 is a peak between 1.8–3.2 μm , but there is less of a unimodal profile owing to what appears to be
584 a secondary mode between 0.56–1.0 μm (Figure 9), which could be linked to some of the non-dust
585 components of vehicular emissions.

586 3.3.5 Waste Processing

587 The final PMF source factor, contributing the least overall to total mass (5.1%), featured
588 Zn, Cd, Pb, Mn, and Cu as its main components. These species are linked to waste processing,
589 including especially electronic waste (e-waste) and battery burning and recycling (Gullett et al.,
590 2007; Iijima et al., 2007), which was previously reported for Manila (Pabroa et al., 2011). The
591 latter study reported that although there are a few licensed operations for battery recycling, there
592 are numerous unregulated cottage melters across Manila that regularly melt metal from batteries
593 and discard the waste freely. Fujimori et al. (2012) additionally showed that e-waste recycling led
594 to emissions of the following elements (in agreement with this PMF cluster) around Metro Manila:
595 Ni, Cu, Pb, Zn, Cd, Ag, In, As, Co, Fe, and Mn.

596 This was the only PMF factor exhibiting comparable weight percentages both below
597 (5.1%) and above 1 μm (5.3%). This is reflected in the mass size distributions of the species
598 included in this cluster being fairly uniformly distributed below and above 1 μm . This is also
599 demonstrated in the reconstructed mass size distribution of this source factor as it clearly exhibits
600 a mode between the other four sources (0.56–1.0 μm) and is the broadest mode (Figure 9). The
601 explanation for this is likely rooted in the diversity of sources contained within this source profile
602 that lead to different sizes of particles. Examples of such sources include processing of different
603 types of waste at varying temperatures and through various processes (e.g., burning, melting,
604 grinding) (Keshtkar and Ashbaugh, 2007),



605 4. Conclusions

606 This study used various analytical techniques (gravimetry, IC, ICP-QQQ, black carbon
607 spectroscopy, and microscopy), meteorological data, and a source apportionment model (PMF) to
608 characterize the sources, chemical composition, and morphology of size-resolved ambient PM in
609 Metro Manila, Philippines during the SWM season of 2018. The main results of this study include
610 the following:

611

- 612 • The total mass concentrations were measured on two occasions and were $18.6 \mu\text{g m}^{-3}$ and 53.0
613 $\mu\text{g m}^{-3}$. Water-soluble mass concentrations were measured on 12 occasions and were on
614 average $8.53 \pm 4.48 \mu\text{g m}^{-3}$ (range = $2.7\text{--}16.6 \mu\text{g m}^{-3}$). Simultaneous measurements of total,
615 water-soluble, and BC mass revealed a composition of 26.9% BC, 31.3% water-soluble
616 components, and 41.8% unaccounted mass.
- 617 • Size-resolved BC mass concentration was measured on one occasion, with the mass sum of all
618 MOUDI stages reaching $14.3 \mu\text{g m}^{-3}$. Most of the BC mass (95%) was contained in the $0.1\text{--}1$
619 μm range (i.e., the Greenfield gap) where wet scavenging by rain is inefficient. The measured
620 BC peaked in the size range of $0.18\text{--}0.32 \mu\text{m}$ and accounted for 51.8% of the measured PM
621 for that stage. In the range of $0.10\text{--}0.18 \mu\text{m}$, the mass percent contribution of BC to the
622 measured PM was 78.1%.
- 623 • Most of the total mass resided in the submicrometer mode ($0.32\text{--}0.56 \mu\text{m}$); however, one
624 MOUDI set revealed an additional supermicrometer mode ($1.8\text{--}3.2 \mu\text{m}$). Water-soluble
625 species that peaked in the submicrometer mode were associated with secondarily produced
626 species, including inorganic acids, amines, MSA, and organic acids. Water-soluble species that
627 peaked in the supermicrometer mode were associated with sea salt and crustal material. Most
628 of the unaccounted mass was for $D_p > 0.32 \mu\text{m}$.
- 629 • The most abundant water-soluble species was SO_4^{2-} ($44\% \pm 6\%$), followed by NH_4^+ ($18\% \pm$
630 5%), NO_3^- ($10 \pm 3\%$), Na^+ ($8 \pm 3\%$), and Cl^- ($6\% \pm 3\%$). Correlation analysis revealed that
631 total water-soluble mass was most correlated with temperature ($r = 0.64$) and rainfall
632 accumulation ($r = -0.49$) among meteorological factors considered, although other factors were
633 likely influential such as wind direction and speed.
- 634 • Regardless of particle size, the majority of single particles examined with SEM-EDX were
635 non-spherical with evidence of agglomeration.



636 • PMF analysis suggested that there were five factors influencing the water-soluble fraction of
637 PM collected at the sampling site. These factors, their contribution to total water-soluble mass,
638 and the main species that permit them to be linked to a physical source are as follows:
639 Aged/Transported (48.0%; NH_4^+ , SO_4^{2-} , MSA, oxalate), Sea Salt (22.5%; Cl^- , NO_3^- , Ca^{2+} , Na^+ ,
640 Mg^{2+} , Ba, Sr), Combustion (18.7%; Ni, As, Co, P, Mo, Cr), Vehicular/Resuspended Dust
641 (5.6%; Al, Ti, Fe), and Waste Processing (5.1%; Zn, Cd, Pb, Mn, Cu). The dominant
642 contribution of Aged/Transported aerosols to water-soluble mass contradicts two expectations:
643 (i) locally-produced sources in polluted cities should drown out the signal of transported
644 aerosols, and (ii) the signal of transported aerosols should be significantly reduced due to
645 scavenging processes upwind of the measurement site.

646

647 Although the current study focuses exclusively on the SWM season in Metro Manila,
648 results of this study are applicable to the study of aerosol impacts on Southeast Asia and other
649 regions. First, the significant presence of Aged/Transported aerosols in Metro Manila indicates
650 that PM in the region has the ability to travel long distances during the SWM season, despite the
651 typical assumption that wet scavenging effectively removes most of the particles. Characterization
652 of aerosols in Metro Manila is therefore important for better understanding the impacts that local
653 emissions will have on locations downwind of Metro Manila, including other populated cities in
654 Southeast and East Asia. Transport of pollution and decreased wet scavenging during the SWM
655 season may become increasingly important as studies have shown a decrease in SWM rainfall and
656 increase in the number of no-rain days during the SWM season in the western Philippines in recent
657 decades (e.g., Cruz et al., 2013).

658 Second, Southeast Asia has been named “one of the most hostile environments on the
659 planet for aerosol remote sensing” (Reid et al., 2013). Therefore, space-based remote sensing of
660 aerosol characteristics, such as retrievals of aerosol optical depth (AOD), in this region are
661 difficult. In situ measurements are critical for characterization of PM in this region, especially
662 during seasons such as the SWM when clouds are especially prevalent and remote-sensing
663 retrievals dependent on clear-sky conditions are lacking.

664 Third, this study provides a valuable dataset to compare to other regions impacted by
665 monsoons where the impacts of enhanced moisture and rainfall on size-resolved composition are
666 not well understood. As aqueous processing results in enhanced production of water-soluble



667 species (e.g., sulfate, organic acids), it is noteworthy for this monsoonal region that the water-
668 soluble fraction remains low relative to BC and other insoluble components. This has major
669 implications for the hygroscopicity of the regional PM.

670 Finally, the results of this study will be used to inform future sampling campaigns in this
671 region, including CAMP²Ex planned for the SWM season of 2019 based in the Philippines. As the
672 current MOUDI sampling campaign at MO is expected to extend for a full year, future work will
673 focus on changes in aerosol characteristics and sources on a seasonal basis.

674
675 *Data availability:* All data used in this work are available upon request.

676
677 *Author Contribution:* MTC, MOC, JBS, ABM, CS, and AS designed the experiments and all co-
678 authors carried out some aspect of the data collection. MTC, RAB, CS, LM, HD, and AS conducted
679 data analysis and interpretation. MTC and AS prepared the manuscript with contributions from all
680 co-authors.

681
682 *Competing interests:* The authors declare that they have no conflict of interest.

683
684 *Acknowledgements:* This research was funded by NASA grant 80NSSC18K0148. M. T. Cruz
685 acknowledges support from the Philippine Department of Science and Technology's ASTHRD
686 Program. R. A. Braun acknowledges support from the ARCS Foundation. A. B. MacDonald
687 acknowledges support from the Mexican National Council for Science and Technology
688 (CONACYT). We acknowledge Agilent Technologies for their support and Shane Snyder's
689 laboratories for ICP-QQQ data.

690
691 **References**

692 Adachi, K., and Tainosho, Y.: Characterization of heavy metal particles embedded in tire dust,
693 Environ Int, 30, 1009-1017, 10.1016/j.envint.2004.04.004, 2004.

694
695 Alas, H. D., Müller, T., Birmili, W., Kecorius, S., Cambaliza, M.O., Simpas, J. B., Cayetano, M.,
696 Weinhold, K., Vallar, E., Galvez, M.C., and Wiedensohler, A.: Spatial Characterization of Black
697 Carbon Mass Concentration in the Atmosphere of a Southeast Asian Megacity: An Air Quality
698 Case Study for Metro Manila, Philippines. Aerosol Air Qual Res. doi.org/10.4209/aaqr.2017.08.0281, 2017.

700



- 701 Allen, H. C., Laux, J. M., Vogt, R., FinlaysonPitts, B. J., and Hemminger, J. C.: Water-induced
702 reorganization of ultrathin nitrate films on NaCl: Implications for the tropospheric chemistry of
703 sea salt particles, *J Phys Chem-Us*, 100, 6371-6375, DOI 10.1021/jp953675a, 1996.
704
- 705 Allen, A. G., Nemitz, E., Shi, J. P., Harrison, R. M., and Greenwood, J. C.: Size distributions of
706 trace metals in atmospheric aerosols in the United Kingdom, *Atmos Environ*, 35, 4581-4591, Doi
707 10.1016/S1352-2310(01)00190-X, 2001.
708
- 709 Almeida, G. P., Bittencourt, A. T., Evangelista, M. S., Vieira-Filho, M. S., and Fornaro, A.:
710 Characterization of aerosol chemical composition from urban pollution in Brazil and its possible
711 impacts on the aerosol hygroscopicity and size distribution, *Atmos Environ*, 202, 149-159,
712 10.1016/j.atmosenv.2019.01.024, 2019.
713
- 714 Anderson, J. R., Aggett, F. J., Buseck, P. R., Germani, M. S., and Shattuck, T. W.: Chemistry of
715 Individual Aerosol-Particles from Chandler, Arizona, an Arid Urban-Environment, *Environ Sci
716 Technol*, 22, 811-818, DOI 10.1021/es00172a011, 1988.
717
- 718 Aswini, A. R., Hegde, P., Nair, P. R., and Aryasree, S.: Seasonal changes in carbonaceous
719 aerosols over a tropical coastal location in response to meteorological processes, *Science of The
720 Total Environment*, 656, 1261-1279, <https://doi.org/10.1016/j.scitotenv.2018.11.366>, 2019.
721
- 722 Bagtasa, G., Cayetano, M. G., and Yuan, C. S.: Seasonal variation and chemical characterization
723 of PM_{2.5} in northwestern Philippines, *Atmos Chem Phys*, 18, 4965-4980, 10.5194/acp-18-4965-
724 2018, 2018.
725
- 726 Bautista, A. T., Pabroa, P. C. B., Santos, F. L., Racho, J. M. D., and Quirit, L. L.: Carbonaceous
727 particulate matter characterization in an urban and a rural site in the Philippines, *Atmos Pollut Res*,
728 5, 245-252, 10.5094/Apr.2014.030, 2014.
729
- 730 Begam, G. R., Vachaspati, C. V., Ahammed, Y. N., Kumar, K. R., Reddy, R. R., Sharma, S. K.,
731 Saxena, M., and Mandal, T. K.: Seasonal characteristics of water-soluble inorganic ions and
732 carbonaceous aerosols in total suspended particulate matter at a rural semi-arid site, Kadapa
733 (India), *Environmental Science and Pollution Research*, 24, 1719-1734, 10.1007/s11356-016-
734 7917-1, 2017.
735
- 736 Behera, S. N., Betha, R., Huang, X., and Balasubramanian, R.: Characterization and estimation of
737 human airway deposition of size-resolved particulate-bound trace elements during a recent haze
738 episode in Southeast Asia, *Environ Sci Pollut R*, 22, 4265-4280, 10.1007/s11356-014-3645-6,
739 2015.
740
- 741 Berresheim, H.: Biogenic Sulfur Emissions from the Sub-Antarctic and Antarctic Oceans, *J
742 Geophys Res-Atmos*, 92, 13245-13262, 10.1029/JD092iD11p13245, 1987.
743
- 744 Braun, R. A., Dadashazar, H., MacDonald, A. B., Aldhaif, A. M., Maudlin, L. C., Crosbie, E.,
745 Aghdam, M. A., Mardi, A. H., and Sorooshian, A.: Impact of Wildfire Emissions on Chloride



- 746 and Bromide Depletion in Marine Aerosol Particles, *Environ Sci Technol*, 51, 9013-9021,
747 10.1021/acs.est.7b02039, 2017.
- 748
- 749 Buchholz, B. A., and Landsberger, S.: Trace-Metal Analysis of Size-Fractioned Municipal Solid-
750 Waste Incinerator Fly-Ash and Its Leachates, *J Environ Sci Heal A*, 28, 423-441, Doi
751 10.1080/10934529309375887, 1993.
- 752
- 753 Burgermeister, S., and Georgii, H. W.: Distribution of Methanesulfonate, Nss Sulfate and
754 Dimethylsulfide over the Atlantic and the North-Sea, *Atmos Environ a-Gen*, 25, 587-595, Doi
755 10.1016/0960-1686(91)90056-D, 1991.
- 756
- 757 Chen, Y. Z., Shah, N., Huggins, F. E., and Huffman, G. P.: Microanalysis of ambient particles
758 from Lexington, KY, by electron microscopy, *Atmos Environ*, 40, 651-663,
759 10.1016/j.atmosenv.2005.09.036, 2006.
- 760
- 761 Chithra, V. S., and Nagendra, S. M. S.: Chemical and morphological characteristics of indoor and
762 outdoor particulate matter in an urban environment, *Atmos Environ*, 77, 579-587,
763 10.1016/j.atmosenv.2013.05.044, 2013.
- 764
- 765 Chuang, M.-T., Chang, S.-C., Lin, N.-H., Wang, J.-L., Sheu, G.-R., Chang, Y.-J., and Lee, C.-T.:
766 Aerosol chemical properties and related pollutants measured in Dongsha Island in the northern
767 South China Sea during 7-SEAS/Dongsha Experiment, *Atmospheric Environment*, 78, 82-92,
768 <https://doi.org/10.1016/j.atmosenv.2012.05.014>, 2013.
- 769
- 770 Clarke, A. D., Shinozuka, Y., Kapustin, V. N., Howell, S., Huebert, B., Doherty, S., Anderson,
771 T., Covert, D., Anderson, J., Hua, X., Moore, K. G., McNaughton, C., Carmichael, G., and
772 Weber, R.: Size distributions and mixtures of dust and black carbon aerosol in Asian outflow:
773 Physiochemistry and optical properties, *J Geophys Res-Atmos*, 109, Artn D15s09
774 10.1029/2003jd004378, 2004.
- 775
- 776 Coggon, M. M., Sorooshian, A., Wang, Z., Metcalf, A. R., Frossard, A. A., Lin, J. J., Craven, J.
777 S., Nenes, A., Jonsson, H. H., Russell, L. M., Flagan, R. C., and Seinfeld, J. H.: Ship impacts on
778 the marine atmosphere: insights into the contribution of shipping emissions to the properties of
779 marine aerosol and clouds, *Atmos Chem Phys*, 12, 8439-8458, 10.5194/acp-12-8439-2012, 2012.
- 780
- 781 Cohen, D. D., Stelcer, E., Santos, F. L., Prior, M., Thompson, C., and Pabroa, P. C. B.:
782 Fingerprinting and source apportionment of fine particle pollution in Manila by IBA and PMF
783 techniques: A 7-year study, *X-Ray Spectrom*, 38, 18-25, 10.1002/xrs.1112, 2009.
- 784
- 785 Crosbie, E., Sorooshian, A., Monfared, N. A., Shingler, T., and Esmaili, O.: A Multi-Year Aerosol
786 Characterization for the Greater Tehran Area Using Satellite, Surface, and Modeling Data,
787 *Atmosphere-Basel*, 5, 178-197, 10.3390/atmos5020178, 2014.
- 788
- 789 Crosbie, E., Youn, J. S., Balch, B., Wonaschutz, A., Shingler, T., Wang, Z., Conant, W. C.,
790 Betterton, E. A., and Sorooshian, A.: On the competition among aerosol number, size and
791 composition in predicting CCN variability: a multi-annual field study in an urbanized desert,
792 *Atmos Chem Phys*, 15, 6943-6958, 10.5194/acp-15-6943-2015, 2015.



- 793
794 Cruz, F. T., Narisma, G. T., Villafuerte, M. Q., Chua, K. U. C., and Olaguera, L. M.: A
795 climatological analysis of the southwest monsoon rainfall in the Philippines, *Atmos Res*, 122, 609-
796 616, 10.1016/j.atmosres.2012.06.010, 2013.
- 797
798 Csavina, J., Landazuri, A., Wonaschutz, A., Rine, K., Rheinheimer, P., Barbaris, B., Conant, W.,
799 Saez, A. E., and Betterton, E. A.: Metal and Metalloid Contaminants in Atmospheric Aerosols
800 from Mining Operations, *Water Air Soil Poll*, 221, 145-157, 10.1007/s11270-011-0777-x, 2011.
801
- 802 Dasgupta, P. K., Campbell, S. W., Al-Horr, R. S., Ullah, S. M. R., Li, J. Z., Amalfitano, C., and
803 Poor, N. D.: Conversion of sea salt aerosol to NaNO_3 and the production of HCl: Analysis of
804 temporal behavior of aerosol chloride/nitrate and gaseous HCl/ HNO_3 concentrations with
805 AIM, *Atmos Environ*, 41, 4242-4257, 10.1016/j.atmosenv.2006.09.054, 2007.
806
- 807 Dumanoglu, Y., Kara, M., Altiok, H., Odabasi, M., Elbir, T., and Bayram, A.: Spatial and seasonal
808 variation and source apportionment of volatile organic compounds (VOCs) in a heavily
809 industrialized region, *Atmos Environ*, 98, 168-178, 10.1016/j.atmosenv.2014.08.048, 2014.
810
- 811 Ervens, B., Sorooshian, A., Aldhaif, A. M., Shingler, T., Crosbie, E., Ziemba, L., Campuzano-
812 Jost, P., Jimenez, J. L., and Wisthaler, A.: Is there an aerosol signature of chemical cloud
813 processing?, *Atmos Chem Phys*, 18, 16099-16119, 10.5194/acp-18-16099-2018, 2018.
814
- 815 Facchini, M. C., Decesari, S., Rinaldi, M., Carbone, C., Finessi, E., Mircea, M., Fuzzi, S.,
816 Moretti, F., Tagliavini, E., Ceburnis, D., and O'Dowd, C. D.: Important Source of Marine
817 Secondary Organic Aerosol from Biogenic Amines, *Environ Sci Technol*, 42, 9116-9121,
818 10.1021/es8018385, 2008.
- 819
820 Farren, N. J., Dunmore, R. E., Mead, M. I., Mohd Nadzir, M. S., Samah, A. A., Phang, S. M.,
821 Bandy, B. J., Sturges, W. T., and Hamilton, J. F.: Chemical characterisation of water-soluble
822 ions in atmospheric particulate matter on the east coast of Peninsular Malaysia, *Atmos. Chem.*
823 *Phys.*, 19, 1537-1553, 10.5194/acp-19-1537-2019, 2019.
- 824
825 Fitzgerald, J. W.: Marine Aerosols - a Review, *Atmos Environ a-Gen*, 25, 533-545, Doi
826 10.1016/0960-1686(91)90050-H, 1991.
- 827
828 Fraser, M. P., Cass, G. R., and Simoneit, B. R. T.: Air quality model evaluation data for organics.
829 6. C-3-C-24 organic acids, *Environ Sci Technol*, 37, 446-453, 10.1021/es0209262, 2003.
830
- 831 Fu, P. Q., Kawamura, K., Chen, J., Li, J., Sun, Y. L., Liu, Y., Tachibana, E., Aggarwal, S. G.,
832 Okuzawa, K., Tanimoto, H., Kanaya, Y., and Wang, Z. F.: Diurnal variations of organic
833 molecular tracers and stable carbon isotopic composition in atmospheric aerosols over Mt. Tai in
834 the North China Plain: an influence of biomass burning, *Atmos Chem Phys*, 12, 8359-8375,
835 10.5194/acp-12-8359-2012, 2012.
- 836
837 Fujimori, T., Takigami, H., Agusa, T., Eguchi, A., Bekki, K., Yoshida, A., Terazono, A., and
838 Ballesteros, F. C.: Impact of metals in surface matrices from formal and informal electronic-



- 839 waste recycling around Metro Manila, the Philippines, and intra-Asian comparison, *J Hazard*
840 *Mater*, 221-222, 139-146, <https://doi.org/10.1016/j.jhazmat.2012.04.019>, 2012.
- 841
- 842 Ge, X. L., Wexler, A. S., and Clegg, S. L.: Atmospheric amines - Part I. A review, *Atmos Environ*,
843 45, 524-546, 10.1016/j.atmosenv.2010.10.012, 2011.
- 844
- 845 Gietl, J. K., Lawrence, R., Thorpe, A. J., and Harrison, R. M.: Identification of brake wear particles
846 and derivation of a quantitative tracer for brake dust at a major road, *Atmos Environ*, 44, 141-146,
847 10.1016/j.atmosenv.2009.10.016, 2010.
- 848
- 849 Gullett, B. K., Linak, W. P., Touati, A., Wasson, S. J., Gatica, S., and King, C. J.: Characterization
850 of air emissions and residual ash from open burning of electronic wastes during simulated
851 rudimentary recycling operations, *J Mater Cycles Waste*, 9, 69-79, 10.1007/s10163-006-0161-x,
852 2007.
- 853
- 854 Harrison, R. M., Beddows, D. C. S., and Dall'Osto, M.: PMF Analysis of Wide-Range Particle
855 Size Spectra Collected on a Major Highway, *Environ Sci Technol*, 45, 5522-5528,
856 10.1021/es2006622, 2011.
- 857
- 858 Harrison, R. M., Jones, A. M., Gietl, J., Yin, J. X., and Green, D. C.: Estimation of the
859 Contributions of Brake Dust, Tire Wear, and Resuspension to Nonexhaust Traffic Particles
860 Derived from Atmospheric Measurements, *Environ Sci Technol*, 46, 6523-6529,
861 10.1021/es300894r, 2012.
- 862
- 863 Hitzenberger, R., and Tohno, S.: Comparison of black carbon (BC) aerosols in two urban areas –
864 concentrations and size distributions, *Atmospheric Environment*, 35, 2153-2167,
865 [https://doi.org/10.1016/S1352-2310\(00\)00480-5](https://doi.org/10.1016/S1352-2310(00)00480-5), 2001.
- 866
- 867 Hopke, P. K., Cohen, D. D., Begum, B. A., Biswas, S. K., Ni, B., Pandit, G. G., Santoso, M.,
868 Chung, Y. S., Davy, P., Markwitz, A., Waheed, S., Siddique, N., Santos, F. L., Pabroa, P. C. B.,
869 Seneviratne, M. C. S., Wimolwattanapun, W., Bunprapob, S., Vuong, T. B., Duy Hien, P. and
870 Markowicz, A.: Urban air quality in the Asian region, *Sci. Total Environ.*, 404(1), 103–112,
871 doi:10.1016/j.scitotenv.2008.05.039, 2008.
- 872
- 873 Huang, S. L., Rahn, K. A., and Arimoto, R.: Testing and optimizing two factor-analysis techniques
874 on aerosol at Narragansett, Rhode Island, *Atmos Environ*, 33, 2169-2185, Doi 10.1016/S1352-
875 2310(98)00324-0, 1999.
- 876
- 877 Iijima, A., Sato, K., Yano, K., Tago, H., Kato, M., Kimura, H., and Furuta, N.: Particle size and
878 composition distribution analysis of automotive brake abrasion dusts for the evaluation of
879 antimony sources of airborne particulate matter, *Atmos Environ*, 41, 4908-4919,
880 10.1016/j.atmosenv.2007.02.005, 2007.
- 881
- 882 Kahnert, M., Nousiainen, T., and Veihelmann, B.: Spherical and spheroidal model particles as an
883 error source in aerosol climate forcing and radiance computations: A case study for feldspar
884 aerosols, *J Geophys Res-Atmos*, 110, Artn D18s13, 10.1029/2004jd005558, 2005.
- 885



- 886 Kautzman, K. E., Surratt, J. D., Chan, M. N., Chan, A. W. H., Hersey, S. P., Chhabra, P. S.,
887 Dalleska, N. F., Wennberg, P. O., Flagan, R. C., and Seinfeld, J. H.: Chemical Composition of
888 Gas- and Aerosol-Phase Products from the Photooxidation of Naphthalene, *J Phys Chem A*, 114,
889 913-934, [10.1021/jp908530s](https://doi.org/10.1021/jp908530s), 2010.
- 890
891 Kawamura, K., and Ikushima, K.: Seasonal-Changes in the Distribution of Dicarboxylic-Acids in
892 the Urban Atmosphere, *Environ Sci Technol*, 27, 2227-2235, DOI [10.1021/es00047a033](https://doi.org/10.1021/es00047a033), 1993.
- 893
894 Kawamura, K., and Kaplan, I. R.: Motor Exhaust Emissions as a Primary Source for Dicarboxylic-
895 Acids in Los-Angeles Ambient Air, *Environ Sci Technol*, 21, 105-110, DOI
896 [10.1021/es00155a014](https://doi.org/10.1021/es00155a014), 1987.
- 897
898 Kawamura, K., and Sakaguchi, F.: Molecular distributions of water soluble dicarboxylic acids in
899 marine aerosols over the Pacific Ocean including tropics, *J Geophys Res-Atmos*, 104, 3501-3509,
900 Doi [10.1029/1998jd100041](https://doi.org/10.1029/1998jd100041), 1999.
- 901
902 Kecorius, S., Madueño, L., Löndahl, J., Vallar, E., Galvez, M. C., Idolor, L. F., Gonzaga-
903 Cayetano, M., Müller, T., Birmili, W., and Wiedensohler, A.: Respiratory tract deposition of
904 inhaled roadside ultrafine refractory particles in a polluted megacity of South-East Asia, *Science*
905 *of The Total Environment*, 663, 265-274, <https://doi.org/10.1016/j.scitotenv.2019.01.338>, 2019.
- 906
907 Kecorius, S., Madueno, L., Vallar, E., Alas, H., Betito, G., Birmili, W., Cambaliza, M. O., Catipay,
908 G., Gonzaga-Cayetano, M., Galvez, M. C., Lorenzo, G., Muller, T., Simpas, J. B., Tamayo, E. G.,
909 and Wiedensohler, A.: Aerosol particle mixing state, refractory particle number size distributions
910 and emission factors in a polluted urban environment: Case study of Metro Manila, Philippines,
911 *Atmos Environ*, 170, 169-183, [10.1016/j.atmosenv.2017.09.037](https://doi.org/10.1016/j.atmosenv.2017.09.037), 2017.
- 912
913 Keshtkar, H., and Ashbaugh, L. L.: Size distribution of polycyclic aromatic hydrocarbon
914 particulate emission factors from agricultural burning, *Atmos Environ*, 41, 2729-2739,
915 [10.1016/j.atmosenv.2006.11.043](https://doi.org/10.1016/j.atmosenv.2006.11.043), 2007.
- 916
917 Kim Oanh, N. T., Upadhyay, N., Zhuang, Y. H., Hao, Z. P., Murthy, D. V. S., Lestari, P., Villarin,
918 J. T., Chengchua, K., Co, H. X., Dung, N. T. and Lindgren, E. S.: Particulate air pollution in six
919 Asian cities: Spatial and temporal distributions, and associated sources, *Atmos. Environ.*, 40(18),
920 3367–3380, doi:[10.1016/j.atmosenv.2006.01.050](https://doi.org/10.1016/j.atmosenv.2006.01.050), 2006.
- 921
922 Kleindienst, T. E., Jaoui, M., Lewandowski, M., Offenber, J. H., and Docherty, K. S.: The
923 formation of SOA and chemical tracer compounds from the photooxidation of naphthalene and its
924 methyl analogs in the presence and absence of nitrogen oxides, *Atmos Chem Phys*, 12, 8711-8726,
925 [10.5194/acp-12-8711-2012](https://doi.org/10.5194/acp-12-8711-2012), 2012.
- 926
927 Liao, H., Chen, W. T., and Seinfeld, J. H.: Role of climate change in global predictions of future
928 tropospheric ozone and aerosols, *J Geophys Res-Atmos*, 111, Artn D12304,
929 [10.1029/2005jd006852](https://doi.org/10.1029/2005jd006852), 2006.
- 930



- 931 Lin, C. C., Chen, S. J., Huang, K. L., Hwang, W. I., Chang-Chien, G. P., and Lin, W. Y.:
932 Characteristics of metals in nano/ultrafine/fine/coarse particles collected beside a heavily
933 trafficked road, *Environ Sci Technol*, 39, 8113-8122, 10.1021/es048182a, 2005.
934
- 935 Linak, W. P., and Miller, C. A.: Comparison of particle size distributions and elemental
936 partitioning from the combustion of pulverized coal and residual fuel oil, *J Air Waste Manage*, 50,
937 1532-1544, Doi 10.1080/10473289.2000.10464171, 2000.
938
- 939 Ma, Y., Li, S., Zheng, J., Khalizov, A., Wang, X., Wang, Z., and Zhou, Y.: Size-resolved
940 measurements of mixing state and cloud-nucleating ability of aerosols in Nanjing, China, *Journal*
941 *of Geophysical Research: Atmospheres*, 122, 9430-9450, 10.1002/2017jd026583, 2017.
942
- 943 Mahowald, N., Jickells, T. D., Baker, A. R., Artaxo, P., Benitez-Nelson, C. R., Bergametti, G.,
944 Bond, T. C., Chen, Y., Cohen, D. D., Herut, B., Kubilay, N., Losno, R., Luo, C., Maenhaut, W.,
945 McGee, K. A., Okin, G. S., Siefert, R. L., and Tsukuda, S.: Global distribution of atmospheric
946 phosphorus sources, concentrations and deposition rates, and anthropogenic impacts, *Global*
947 *Biogeochem Cy*, 22, 10.1029/2008gb003240, 2008.
948
- 949 Marple, V., Olson, B., Romay, F., Hudak, G., Geerts, S. M. and Lundgren, D.: Second generation
950 micro-orifice uniform deposit impactor, 120 MOUDI-II: Design, Evaluation, and application to
951 long-term ambient sampling, *Aerosol Sci. Technol.*, 48(4), 427-433,
952 doi:10.1080/02786826.2014.884274, 2014.
953
- 954 Martens, C. S., Wesolowski, J. J., Harriss, R. C., and Kaifer, R.: Chlorine Loss from Puerto-Rican
955 and San-Francisco-Bay Area Marine Aerosols, *J Geophys Res*, 78, 8778-8792, DOI
956 10.1029/JC078i036p08778, 1973.
957
- 958 Maudlin, L. C., Wang, Z., Jonsson, H. H., and Sorooshian, A.: Impact of wildfires on size-
959 resolved aerosol composition at a coastal California site, *Atmos Environ*, 119, 59-68,
960 10.1016/j.atmosenv.2015.08.039, 2015.
961
- 962 Metcalf, A. R., Craven, J. S., Ensberg, J. J., Brioude, J., Angevine, W., Sorooshian, A., Duong,
963 H. T., Jonsson, H. H., Flagan, R. C., and Seinfeld, J. H.: Black carbon aerosol over the Los
964 Angeles Basin during CalNex, *J Geophys Res-Atmos*, 117, 10.1029/2011jd017255, 2012.
965
- 966 Mielonen, T., Levy, R. C., Aaltonen, V., Komppula, M., de Leeuw, G., Huttunen, J., Lihavainen,
967 H., Kolmonen, P., Lehtinen, K. E. J., and Arola, A.: Evaluating the assumptions of surface
968 reflectance and aerosol type selection within the MODIS aerosol retrieval over land: the problem
969 of dust type selection, *Atmos Meas Tech*, 4, 201-214, 10.5194/amt-4-201-2011, 2011.
970
- 971 Miller, J., and Miller, J.C.: *Statistics and chemometrics for analytical chemistry*. Pearson
972 Education, 2018.
973
- 974 Mishra, S. K., Agnihotri, R., Yadav, P. K., Singh, S., Prasad, M. V. S. N., Praveen, P. S., Tawale,
975 J. S., Rashmi, Mishra, N. D., Arya, B. C., and Sharma, C.: Morphology of Atmospheric Particles
976 over Semi-Arid Region (Jaipur, Rajasthan) of India: Implications for Optical Properties, *Aerosol*
977 *Air Qual Res*, 15, 974+, 10.4209/aaqr.2014.10.0244, 2015.



- 978
979 Mooibroek, D., Schaap, M., Weijers, E. P., and Hoogerbrugge, R.: Source apportionment and
980 spatial variability of PM_{2.5} using measurements at five sites in the Netherlands, *Atmospheric*
981 *Environment*, 45, 4180-4191, 10.1016/j.atmosenv.2011.05.017, 2011.
982
983 Mosier, A. R., Andre, C. E., and Viets, F. G.: Identification of Aliphatic-Amines Volatilized from
984 Cattle Feedyard, *Environ Sci Technol*, 7, 642-644, DOI 10.1021/es60079a009, 1973.
985
986 Muller, C., Inuma, Y., Karstensen, J., van Pinxteren, D., Lehmann, S., Gnauk, T., and Herrmann,
987 H.: Seasonal variation of aliphatic amines in marine sub-micrometer particles at the Cape Verde
988 islands, *Atmos Chem Phys*, 9, 9587-9597, 2009.
989
990 Murphy, S. M., Agrawal, H., Sorooshian, A., Padro, L. T., Gates, H., Hersey, S., Welch, W. A.,
991 Jung, H., Miller, J. W., Cocker, D. R., Nenes, A., Jonsson, H. H., Flagan, R. C., and Seinfeld, J.
992 H.: Comprehensive Simultaneous Shipboard and Airborne Characterization of Exhaust from a
993 Modern Container Ship at Sea, *Environ Sci Technol*, 43, 4626-4640, 10.1021/es802413j, 2009.
994
995 Norris, G., Duvall, R., Brown, S., and Bai, S.: EPA Positive Matrix Factorization (PMF) 5.0
996 fundamentals and User Guide Prepared for the US Environmental Protection Agency Office of
997 Research and Development, Washington, DC. Inc., Petaluma, 2014.
998
999 Nriagu, J. O.: A Global Assessment of Natural Sources of Atmospheric Trace-Metals, *Nature*, 338,
1000 47-49, DOI 10.1038/338047a0, 1989.
1001
1002 Pabroa, P. C. B., Santos, F. L., Morco, R. P., Racho, J. M. D., Bautista, A. T., and Bucal, C. G. D.:
1003 Receptor modeling studies for the characterization of air particulate lead pollution sources in
1004 Valenzuela sampling site (Philippines), *Atmos Pollut Res*, 2, 213-218, 10.5094/Apr.2011.027,
1005 2011.
1006
1007 Philippine Statistics Authority: <https://psa.gov.ph/>, Accessed 28 August 2018.
1008
1009 Polissar, A., Hopke, P., Paatero, P., Malm, W., and Sisler, J.: Atmospheric aerosol over Alaska 2.
1010 Elemental composition and sources. *Journal of Geophysical Research* 103, 19045-19057, 1998.
1011
1012 Prabhakar, G., Ervens, B., Wang, Z., Maudlin, L. C., Coggon, M. M., Jonsson, H. H., Seinfeld, J.
1013 H., and Sorooshian, A.: Sources of nitrate in stratocumulus cloud water: Airborne measurements
1014 during the 2011 E-PEACE and 2013 NiCE studies, *Atmos Environ*, 97, 166-173,
1015 10.1016/j.atmosenv.2014.08.019, 2014a.
1016
1017 Prabhakar, G., Sorooshian, A., Toffol, E., Arellano, A. F., and Betterton, E. A.: Spatiotemporal
1018 distribution of airborne particulate metals and metalloids in a populated arid region, *Atmos*
1019 *Environ*, 92, 339-347, 10.1016/j.atmosenv.2014.04.044, 2014b.
1020
1021 Qu, W. J., Wang, J., Zhang, X. Y., Wang, D., and Sheng, L. F.: Influence of relative humidity on
1022 aerosol composition: Impacts on light extinction and visibility impairment at two sites in coastal
1023 area of China, *Atmos Res*, 153, 500-511, 10.1016/j.atmosres.2014.10.009, 2015.
1024



- 1025 Raatikainen, T., Brus, D., Hyvärinen, A. P., Svensson, J., Asmi, E., and Lihavainen, H.: Black
1026 carbon concentrations and mixing state in the Finnish Arctic, *Atmos. Chem. Phys.*, 15, 10057-
1027 10070, 10.5194/acp-15-10057-2015, 2015.
1028
- 1029 Ramachandran, S., and Rajesh, T. A.: Black carbon aerosol mass concentrations over
1030 Ahmedabad, an urban location in western India: Comparison with urban sites in Asia, Europe,
1031 Canada, and the United States, *J Geophys Res-Atmos*, 112, 10.1029/2006jd007488, 2007.
1032
- 1033 Ran, L., Deng, Z. Z., Wang, P. C., and Xia, X. A.: Black carbon and wavelength-dependent aerosol
1034 absorption in the North China Plain based on two-year aethalometer measurements, *Atmos*
1035 *Environ*, 142, 132-144, 10.1016/j.atmosenv.2016.07.014, 2016.
1036
- 1037 Reddington, C. L., McMeeking, G., Mann, G. W., Coe, H., Frontoso, M. G., Liu, D., Flynn, M.,
1038 Spracklen, D. V., and Carslaw, K. S.: The mass and number size distributions of black carbon
1039 aerosol over Europe, *Atmos. Chem. Phys.*, 13, 4917-4939, 10.5194/acp-13-4917-2013, 2013.
1040
- 1041 Reff, A., Eberly, S.I., and Bhave, P.V.: Receptor modeling of ambient particulate matter data using
1042 positive matrix factorization: Review of existing methods. *J Air Waste Manage* 57, 146-154, 2007.
1043
- 1044 Reid, J. S., Xian, P., Hyer, E. J., Flatau, M. K., Ramirez, E. M., Turk, F. J., Sampson, C. R., Zhang,
1045 C., Fukada, E. M., and Maloney, E. D.: Multi-scale meteorological conceptual analysis of observed
1046 active fire hotspot activity and smoke optical depth in the Maritime Continent, *Atmos Chem Phys*,
1047 12, 2117-2147, 10.5194/acp-12-2117-2012, 2012.
1048
- 1049 Reid, J. S., Hyer, E. J., Johnson, R. S., Holben, B. N., Yokelson, R. J., Zhang, J. L., Campbell, J.
1050 R., Christopher, S. A., Di Girolamo, L., Giglio, L., Holz, R. E., Kearney, C., Miettinen, J., Reid,
1051 E. A., Turk, F. J., Wang, J., Xian, P., Zhao, G. Y., Balasubramanian, R., Chew, B. N., Janjai, S.,
1052 Lagrosas, N., Lestari, P., Lin, N. H., Mahmud, M., Nguyen, A. X., Norris, B., Oanh, N. T. K., Oo,
1053 M., Salinas, S. V., Welton, E. J., and Liew, S. C.: Observing and understanding the Southeast
1054 Asian aerosol system by remote sensing: An initial review and analysis for the Seven Southeast
1055 Asian Studies (7SEAS) program, *Atmos Res*, 122, 403-468, 10.1016/j.atmosres.2012.06.005,
1056 2013.
1057
- 1058 Reid, J. S., Xian, P., Holben, B. N., Hyer, E. J., Reid, E. A., Salinas, S. V., Zhang, J. L., Campbell,
1059 J. R., Chew, B. N., Holz, R. E., Kuciauskas, A. P., Lagrosas, N., Posselt, D. J., Sampson, C. R.,
1060 Walker, A. L., Welton, E. J., and Zhang, C. D.: Aerosol meteorology of the Maritime Continent
1061 for the 2012 7SEAS southwest monsoon intensive study - Part 1: regional-scale phenomena,
1062 *Atmos Chem Phys*, 16, 14041-14056, 10.5194/acp-16-14041-2016, 2016a.
1063
- 1064 Reid, J. S., Lagrosas, N. D., Jonsson, H. H., Reid, E. A., Atwood, S. A., Boyd, T. J., Ghate, V. P.,
1065 Xian, P., Posselt, D. J., Simpas, J. B., Uy, S. N., Zaiger, K., Blake, D. R., Bucholtz, A., Campbell,
1066 J. R., Chew, B. N., Cliff, S. S., Holben, B. N., Holz, R. E., Hyer, E. J., Kreidenweis, S. M.,
1067 Kuciauskas, A. P., Lolli, S., Oo, M., Perry, K. D., Salinas, S. V., Sessions, W. R., Smirnov, A.,
1068 Walker, A. L., Wang, Q., Yu, L. Y., Zhang, J. L., and Zhao, Y. J.: Aerosol meteorology of
1069 Maritime Continent for the 2012 7SEAS southwest monsoon intensive study - Part 2: Philippine



- 1070 receptor observations of fine-scale aerosol behavior, *Atmos Chem Phys*, 16, 14057-14078,
1071 10.5194/acp-16-14057-2016, 2016b.
- 1072
- 1073 Rocha, L. D. S., and Correa, S. M.: Determination of size-segregated elements in diesel-biodiesel
1074 blend exhaust emissions, *Environ Sci Pollut R*, 25, 18121-18129, 10.1007/s11356-018-1980-8,
1075 2018.
- 1076
- 1077 Rogge, W. F., Mazurek, M. A., Hildemann, L. M., Cass, G. R., and Simoneit, B. R. T.:
1078 Quantification of Urban Organic Aerosols at a Molecular-Level - Identification, Abundance and
1079 Seasonal-Variation, *Atmos Environ a-Gen*, 27, 1309-1330, Doi 10.1016/0960-1686(93)90257-Y,
1080 1993.
- 1081
- 1082 Ro, C. U., Oh, K. Y., Kim, H., Kim, Y. P., Lee, C. B., Kim, K. H., Kang, C. H., Osan, J., De
1083 Hoog, J., Worobiec, A., and Van Grieken, R.: Single-particle analysis of aerosols at Cheju
1084 Island, Korea, using low-Z electron probe X-ray microanalysis: A direct proof of nitrate
1085 formation from sea salts, *Environ Sci Technol*, 35, 4487-4494, 10.1021/es0155231, 2001.
- 1086
- 1087 Rolph, G.D.: Real-time Environmental Applications and Display sYstem (READY) website
1088 (<http://ready.Arl.NOAA.Gov>), NOAA Air Resour. Lab., Silver Spring, Md., 2016.
- 1089
- 1090 Roth, B., and Okada, K.: On the modification of sea-salt particles in the coastal atmosphere,
1091 *Atmos Environ*, 32, 1555-1569, Doi 10.1016/S1352-2310(97)00378-6, 1998.
- 1092
- 1093 Saltzman, E. S., Savoie, D. L., Zika, R. G., and Prospero, J. M.: Methane Sulfonic-Acid in the
1094 Marine Atmosphere, *J Geophys Res-Oceans*, 88, 897-902, DOI 10.1029/JC088iC15p10897, 1983.
- 1095
- 1096 Saltzman, E. S., Savoie, D. L., Prospero, J. M., and Zika, R. G.: Methanesulfonic-Acid and Non-
1097 Sea-Salt Sulfate in Pacific Air - Regional and Seasonal-Variations, *J Atmos Chem*, 4, 227-240,
1098 Doi 10.1007/Bf00052002, 1986.
- 1099
- 1100 Schade, G. W., and Crutzen, P. J.: Emission of Aliphatic-Amines from Animal Husbandry and
1101 Their Reactions - Potential Source of N₂O and HCN, *J Atmos Chem*, 22, 319-346, Doi
1102 10.1007/Bf00696641, 1995.
- 1103
- 1104 Schwarz, J. P., Gao, R. S., Spackman, J. R., Watts, L. A., Thomson, D. S., Fahey, D. W., Ryerson,
1105 T. B., Peischl, J., Holloway, J. S., Trainer, M., Frost, G. J., Baynard, T., Lack, D. A., de Gouw, J.
1106 A., Warneke, C., and Del Negro, L. A.: Measurement of the mixing state, mass, and optical size
1107 of individual black carbon particles in urban and biomass burning emissions, *Geophysical
1108 Research Letters*, 35, 10.1029/2008gl033968, 2008.
- 1109
- 1110 Seinfeld, J. H., and Pandis, S. N.: *Atmospheric chemistry and physics* (3rd ed.). New York: Wiley-
1111 Interscience, 2016.
- 1112
- 1113 Shafer, M. M., Toner, B. M., Oyerdier, J. T., Schauer, J. J., Fakra, S. C., Hu, S. H., Herner, J. D.,
1114 and Ayala, A.: Chemical Speciation of Vanadium in Particulate Matter Emitted from Diesel



- 1115 Vehicles and Urban Atmospheric Aerosols, *Environ Sci Technol*, 46, 189-195,
1116 10.1021/es200463c, 2012.
- 1117
- 1118 Shingler, T., Sorooshian, A., Ortega, A., Crosbie, E., Wonaschutz, A., Perring, A. E.,
1119 Beyersdorf, A., Ziemba, L., Jimenez, J. L., Campuzano-Jost, P., Mikoviny, T., Wisthaler, A., and
1120 Russell, L. M.: Ambient observations of hygroscopic growth factor and $f(\text{RH})$ below 1: Case
1121 studies from surface and airborne measurements, *J Geophys Res-Atmos*, 121, 13661-13677,
1122 10.1002/2016jd025471, 2016.
- 1123
- 1124 Shiraiwa, M., Kondo, Y., Moteki, N., Takegawa, N., Sahu, L. K., Takami, A., Hatakeyama, S.,
1125 Yonemura, S., and Blake, D. R.: Radiative impact of mixing state of black carbon aerosol in Asian
1126 outflow, *Journal of Geophysical Research: Atmospheres*, 113, 10.1029/2008jd010546, 2008.
- 1127
- 1128 Simpas, J., Lorenzo, G., and Cruz, M. T.: Monitoring Particulate Matter Levels and Composition
1129 for Source Apportionment Study in Metro Manila, Philippines, in: *Improving Air Quality in Asian
1130 Developing Countries: Compilation of Research Findings*, Kim Oanh, N. T. (Ed.), NARENCA,
1131 Vietnam Publishing House of Natural Resources, Environment and Cartography, Vietnam, 239-
1132 261, 2014.
- 1133
- 1134 Singh, M., Jaques, P. A., and Sioutas, C.: Size distribution and diurnal characteristics of particle-
1135 bound metals in source and receptor sites of the Los Angeles Basin, *Atmos Environ*, 36, 1675-
1136 1689, Pii S1352-2310(02)00166-8, Doi 10.1016/S1352-2310(02)00166-8, 2002.
- 1137
- 1138 Song, F., and Gao, Y.: Size distributions of trace elements associated with ambient particular
1139 matter in the affinity of a major highway in the New Jersey-New York metropolitan area, *Atmos
1140 Environ*, 45, 6714-6723, 10.1016/j.atmosenv.2011.08.031, 2011.
- 1141
- 1142 Sorooshian, A., Ng, N. L., Chan, A. W. H., Feingold, G., Flagan, R. C., and Seinfeld, J. H.:
1143 Particulate organic acids and overall water-soluble aerosol composition measurements from the
1144 2006 Gulf of Mexico Atmospheric Composition and Climate Study (GoMACCS), *J Geophys
1145 Res-Atmos*, 112, 10.1029/2007jd008537, 2007.
- 1146
- 1147 Sorooshian, A., Murphy, S. N., Hersey, S., Gates, H., Padro, L. T., Nenes, A., Brechtel, F. J.,
1148 Jonsson, H., Flagan, R. C., and Seinfeld, J. H.: Comprehensive airborne characterization of aerosol
1149 from a major bovine source, *Atmos Chem Phys*, 8, 5489-5520, DOI 10.5194/acp-8-5489-2008,
1150 2008.
- 1151
- 1152 Sorooshian, A., Padro, L. T., Nenes, A., Feingold, G., McComiskey, A., Hersey, S. P., Gates, H.,
1153 Jonsson, H. H., Miller, S. D., Stephens, G. L., Flagan, R. C., and Seinfeld, J. H.: On the link
1154 between ocean biota emissions, aerosol, and maritime clouds: Airborne, ground, and satellite
1155 measurements off the coast of California, *Global Biogeochem Cy*, 23,
1156 10.1029/2009gb003464, 2009.
- 1157
- 1158 Sorooshian, A., Crosbie, E., Maudlin, L. C., Youn, J. S., Wang, Z., Shingler, T., Ortega, A. M.,
1159 Hersey, S., and Woods, R. K.: Surface and airborne measurements of organosulfur and
1160 methanesulfonate over the western United States and coastal areas, *J Geophys Res-Atmos*, 120,
1161 8535-8548, 10.1002/2015jd023822, 2015.



- 1162
1163 Stein, A. F., Draxler, R. R., Rolph, G. D., Stunder, B. J. B., Cohen, M. D., and Ngan, F.: NOAA's
1164 Hysplit Atmospheric Transport and Dispersion Modeling System, *B Am Meteorol Soc*, 96, 2059-
1165 2077, 10.1175/Bams-D-14-00110.1, 2015.
1166
1167 Tai, A. P. K., Mickley, L. J., and Jacob, D. J.: Correlations between fine particulate matter (PM_{2.5})
1168 and meteorological variables in the United States: Implications for the sensitivity of PM_{2.5} to
1169 climate change, *Atmos Environ*, 44, 3976-3984, 10.1016/j.atmosenv.2010.06.060, 2010.
1170
1171 Tsakalou, C., Papamarkou, S., Tsakiridis, P. E., Bartzas, G., and Tsakalakis, K.: Characterization
1172 and leachability evaluation of medical wastes incineration fly and bottom ashes and their
1173 vitrification outgrowths, *J Environ Chem Eng*, 6, 367-376, 10.1016/j.jece.2017.12.012, 2018.
1174
1175 VandenBoer, T. C., Petroff, A., Markovic, M. Z., and Murphy, J. G.: Size distribution of alkyl
1176 amines in continental particulate matter and their online detection in the gas and particle phase,
1177 *Atmos Chem Phys*, 11, 4319-4332, 10.5194/acp-11-4319-2011, 2011.
1178
1179 Villafuerte, M. Q., Matsumoto, J., Akasaka, I., Takahashi, H. G., Kubota, H., and Cinco, T. A.:
1180 Long-term trends and variability of rainfall extremes in the Philippines, *Atmos Res*, 137, 1-13,
1181 10.1016/j.atmosres.2013.09.021, 2014.
1182
1183 Vossler, T., Cernikovskiy, L., Novak, J., and Williams, R.: Source apportionment with
1184 uncertainty estimates of fine particulate matter in Ostrava, Czech Republic using Positive Matrix
1185 Factorization, *Atmos Pollut Res*, 7, 503-512, 10.1016/j.apr.2015.12.004, 2016.
1186
1187 Wang, J., Ge, C., Yang, Z. F., Hyer, E. J., Reid, J. S., Chew, B. N., Mahmud, M., Zhang, Y. X.,
1188 and Zhang, M. G.: Mesoscale modeling of smoke transport over the Southeast Asian Maritime
1189 Continent: Interplay of sea breeze, trade wind, typhoon, and topography, *Atmos Res*, 122, 486-
1190 503, 10.1016/j.atmosres.2012.05.009, 2013.
1191
1192 Wang, Y. Q., Zhang, X. Y., and Draxler, R. R.: TrajStat: GIS-based software that uses various
1193 trajectory statistical analysis methods to identify potential sources from long-term air pollution
1194 measurement data, *Environ Modell Softw*, 24, 938-939, 10.1016/j.envsoft.2009.01.004, 2009.
1195
1196 Wasson, S. J., Linak, W. P., Gullett, B. K., King, C. J., Touati, A., Huggins, F. E., Chen, Y. Z.,
1197 Shah, N., and Huffman, G. P.: Emissions of chromium, copper, arsenic, and PCDDs/Fs from open
1198 burning of CCA-treated wood, *Environ Sci Technol*, 39, 8865-8876, 10.1021/es050891g, 2005.
1199
1200 Watson, J. G.: Protocol for Applying and Validating the CMB Model for PM_{2.5} and VOC. Report
1201 No. EPA-451/R-04-001. US Environmental Protection Agency, Research Triangle Park, NC.,
1202 2004.
1203
1204 Watts, S. F., Watson, A., and Brimblecombe, P.: Measurements of the Aerosol Concentrations of
1205 Methanesulfonic Acid, Dimethyl-Sulfoxide and Dimethyl Sulfone in the Marine Atmosphere of
1206 the British-Isles, *Atmos Environ*, 21, 2667-2672, Doi 10.1016/0004-6981(87)90198-3, 1987.
1207



- 1208 Wonaschuetz, A., Sorooshian, A., Ervens, B., Chuang, P. Y., Feingold, G., Murphy, S. M., de
1209 Gouw, J., Warneke, C., and Jonsson, H. H.: Aerosol and gas re-distribution by shallow cumulus
1210 clouds: An investigation using airborne measurements, *J Geophys Res-Atmos*, 117,
1211 10.1029/2012jd018089, 2012.
1212
- 1213 Wu, D., Zhang, F., Lou, W. H., Li, D., and Chen, J. M.: Chemical characterization and toxicity
1214 assessment of fine particulate matters emitted from the combustion of petrol and diesel fuels, *Sci*
1215 *Total Environ*, 605, 172-179, 10.1016/j.scitotenv.2017.06.058, 2017.
1216
- 1217 Xian, P., Reid, J. S., Atwood, S. A., Johnson, R. S., Hyer, E. J., Westphal, D. L., and Sessions, W.:
1218 Smoke aerosol transport patterns over the Maritime Continent, *Atmos Res*, 122, 469-485,
1219 10.1016/j.atmosres.2012.05.006, 2013.
1220
- 1221 Xu, G. J., and Gao, Y.: Characterization of marine aerosols and precipitation through shipboard
1222 observations on the transect between 31 degrees N-32 degrees S in the West Pacific, *Atmos Pollut*
1223 *Res*, 6, 154-161, 10.5094/Apr.2015.018, 2015.
1224
- 1225 Yao, X. H., Fang, M., and Chan, C. K.: The size dependence of chloride depletion in fine and
1226 coarse sea-salt particles, *Atmos Environ*, 37, 743-751, 10.1016/S1352-2310(02)00955-X, 2003.
1227
- 1228 Youn, J. S., Wang, Z., Wonaschutz, A., Arellano, A., Betterton, E. A., and Sorooshian, A.:
1229 Evidence of aqueous secondary organic aerosol formation from biogenic emissions in the North
1230 American Sonoran Desert, *Geophys Res Lett*, 40, 3468-3472, 10.1002/grl.50644, 2013.
1231
- 1232 Youn, J. S., Crosbie, E., Maudlin, L. C., Wang, Z., and Sorooshian, A.: Dimethylamine as a major
1233 alkyl amine species in particles and cloud water: Observations in semi-arid and coastal regions,
1234 *Atmos Environ*, 122, 250-258, 10.1016/j.atmosenv.2015.09.061, 2015.
1235
- 1236 Youn, J. S., Csavina, J., Rine, K. P., Shingler, T., Taylor, M. P., Saez, A. E., Betterton, E. A., and
1237 Sorooshian, A.: Hygroscopic Properties and Respiratory System Deposition Behavior of
1238 Particulate Matter Emitted By Mining and Smelting Operations, *Environ Sci Technol*, 50, 11706-
1239 11713, 10.1021/acs.est.6b03621, 2016.
1240



1241 **Table 1.** Summary of average operating parameters, meteorological conditions, and total resolved
1242 water-soluble mass concentration for each MOUDI sample set collected at Manila Observatory
1243 (MO) during the 2018 Southwest Monsoon period. On two occasions, simultaneous MOUDI sets
1244 were collected for one set to undergo gravimetric analysis (MO3 and MO13) to compare with mass
1245 resolved from chemical speciation of the water-soluble fraction (MO4 and MO14). One additional
1246 MOUDI set devoted to microscopy analysis was collected using aluminum substrates for one hour
1247 on August 1 at 30 LPM.
1248

Sample set name	Dates	Durat ion (hrs)	Flow rate (LPM)	Wind speed (m/s)	Wind direction (°)	T (°C)	Rain (mm)	Water-soluble mass ($\mu\text{g m}^{-3}$)
MO1	Jul 19-20	24	30	3.3	90.1	24.9	47	4.6
MO2	Jul 23-25	54	30	1.3	95.8	26.7	7.8	6.5
MO3/4	Jul 25-30	119	28/30	1.2	111.8	26.7	49.6	5.2
MO5	Jul 30-Aug 1	42	29	2.6	98.1	27.5	52.8	9.2
MO6	Aug 6-8	48	27	0.9	127.5	26.1	30.4	5.1
MO7	Aug 14-16	48	28	3.0	107.8	27.8	2.8	13.7
MO8	Aug 22-24	48	29	3.5	108.7	28.1	1	12.8
MO9	Sep 1-3	48	27	0.7	98.6	26.6	51.6	6.2
MO10	Sep 10-12	48	29	1.0	94.7	26.2	78.4	6.4
MO11	Sep 18-20	48	27	0.5	290.2	27.8	0	2.7
MO12	Sep 26-28	48	27	1.2	96.3	27.8	6.8	13.5
MO13/14	Oct 6-8	48	28/26	0.6	108.2	27.8	0.8	16.6

1249

1250



1251 **Table 2.** Charge balance slopes (cations on y-axis; anions on x-axis) for the MOUDI sets shown
1252 including the averages of all sets (All) for three size ranges: submicrometer stages spanning 0.056
1253 – 1.0 μm ; supermicrometer stages ($> 1.0 \mu\text{m}$); and all stages ($> 0.056 \mu\text{m}$). The species used in
1254 the charge balance analysis include those speciated with the IC (listed in Section 2.3) plus K from
1255 ICP-QQQ analysis.
1256

Sample set	0.056 – 1.0 μm	$> 1 \mu\text{m}$	$> 0.056 \mu\text{m}$
MO1	0.87	1.37	0.89
MO2	1.46	1.26	1.41
MO4	1.25	1.17	1.21
MO5	1.35	1.43	1.41
MO6	1.29	1.45	1.31
MO7	1.40	1.23	1.36
MO8	1.35	1.33	1.36
MO9	1.28	1.55	1.26
MO10	1.37	1.36	1.35
MO11	0.97	1.60	1.27
MO12	1.37	1.19	1.33
MO14	1.31	1.28	1.29
All	1.35	1.24	1.33

1257
1258



1259 **Table 3.** Contributions (in weight percentage) of each PMF source factor to the total mass in
1260 different diameter ranges.
1261

Diameter Range (μm)	Aged/ Transported	Sea Salt	Combustion	Vehicular/ Resuspended Dust	Waste Processing
> 0.056	48.0%	22.5%	18.7%	5.6%	5.1%
0.056 - 1.0	68.9%	0.6%	23.9%	1.5%	5.1%
> 1.0	18.6%	53.5%	11.3%	11.3%	5.3%

1262



1263 **Table 4.** Correlation matrix (r values) between water-soluble species based on total MOUDI-
 1264 integrated mass concentrations ($> 0.056 \mu\text{m}$). Blank cells represent statistically insignificant
 1265 values. Results for the sub- and supermicrometer ranges are in Tables S2-S3. Panels A-E
 1266 represent important species from each of the source profiles identified in Section 3.3: A =
 1267 Aged/Transported, B = Sea Salt, C = Combustion, D = Vehicular/Resuspended Dust, E = Waste
 1268 Processing. DMA – Dimethylamine, MSA – Methanesulfonate, PH – Phthalate, OX – Oxalate,
 1269 MA – Maleate, SU – Succinate, AD – Adipate.
 1270

A)															
OX	1.00														
SO ₄	0.74	1.00													
NH ₄	0.68	0.99	1.00												
Sn	0.71	0.87	0.85	1.00											
Rb	0.73	0.74	0.73	0.69	1.00										
K	0.76	0.71	0.69	0.69	0.97	1.00									
Cs	0.72	0.82	0.81	0.74	0.96	0.91	1.00								
V	0.36	0.64	0.63	0.48	0.53	0.51	0.57	1.00							
DMA		0.35		0.38	0.45	0.37	0.45		1.00						
MSA	0.71	0.89	0.89	0.79	0.90	0.85	0.92	0.51	0.47	1.00					
PH	0.68	0.67	0.68	0.73	0.82	0.76	0.80		0.38	0.88	1.00				
SU	0.63	0.56	0.59	0.44	0.87	0.81	0.82		0.68	0.78	0.84	1.00			
AD	0.40	0.66	0.70	0.62	0.70	0.70	0.77		0.84	0.74	0.75	0.90	1.00		
Se	0.75	0.75	0.73	0.66	0.80	0.78	0.79	0.32	0.34	0.78	0.80	0.88	0.88	1.00	
Tl	0.75	0.87	0.86	0.80	0.89	0.85	0.94	0.74	0.65	0.80	0.52	0.70		0.43	1.00
	OX	SO ₄	NH ₄	Sn	Rb	K	Cs	V	DMA	MSA	PH	SU	AD	Se	Tl

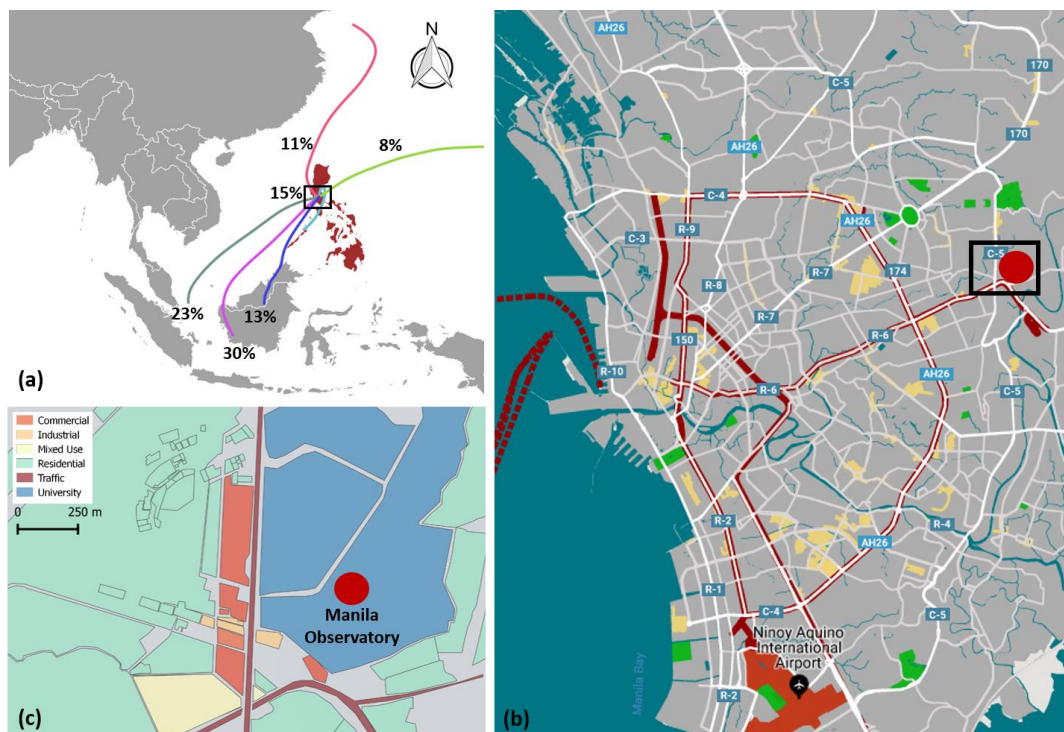
B)								
Cl	1.00							
NO ₃	0.76	1.00						
Ba	0.66	0.80	1.00					
Sr	0.78	0.87	0.91	1.00				
Ca	0.58	0.79	0.75	0.78	1.00			
Na	0.93	0.87	0.75	0.85	0.63	1.00		
Mg	0.91	0.87	0.77	0.87	0.66	0.99	1.00	
Hf					0.57		1.00	
	Cl	NO ₃	Ba	Sr	Ca	Na	Mg	Hf

C)								
As	1.00							
Ni	0.58	1.00						
Co			1.00					
P		0.33	0.34	1.00				
Mo					1.00			
Cr	0.62	0.49		0.20		1.00		
MA			0.67		-0.42		1.00	
Ag			0.85		0.64		1.00	
	As	Ni	Co	P	Mo	Cr	Mal	Ag

D)						
Zr	1.00					
Y	0.75	1.00				
Al	0.88	0.76	1.00			
Fe	0.33	0.61	0.25	1.00		
Ti	0.84	0.66	0.82	0.41	1.00	
Nb	0.70	0.50	0.59	0.59	0.70	1.00
	Zr	Y	Al	Fe	Ti	Nb

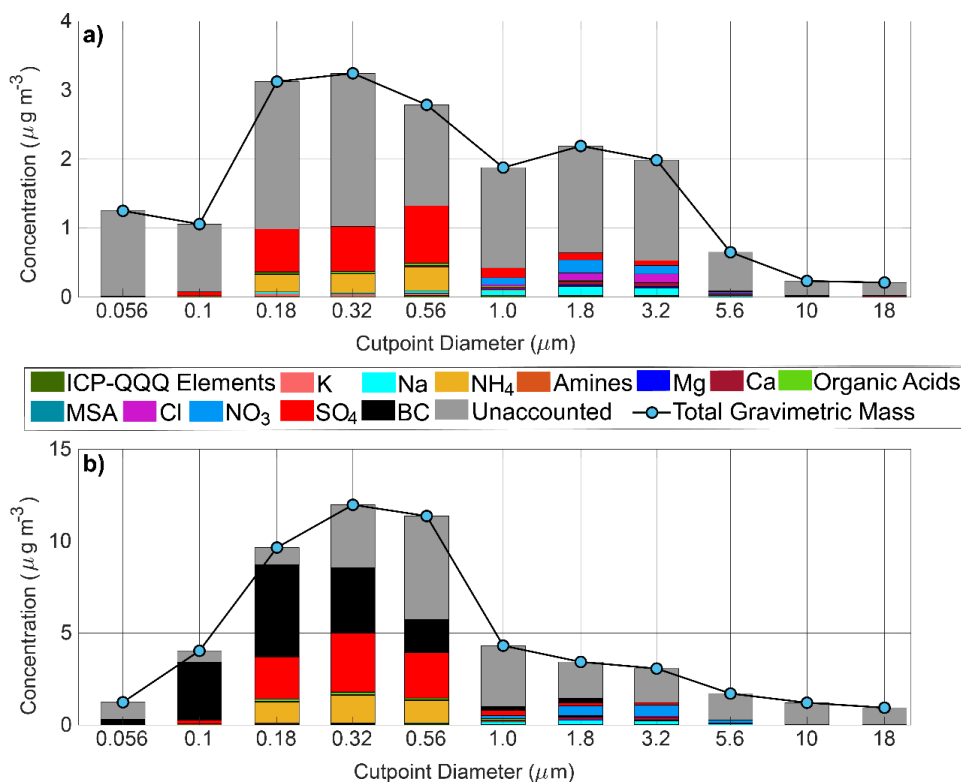
E)					
Cd	1.00				
Zn	0.60	1.00			
Cu	0.21	0.27	1.00		
Mn	0.28	0.61	0.22	1.00	
Pb	0.78	0.58	0.38	0.27	1.00
	Cd	Zn	Cu	Mn	Pb

1271
 1272
 1273
 1274



1275
1276 **Figure 1.** (a) Location of Metro Manila, Philippines relative to Southeast Asia. Also shown are
1277 5-day backward trajectory frequencies during the sampling duration based on HYSPLIT cluster
1278 analysis; note that 15% correspond to trajectories within the black square. (b) Close-up view of
1279 Metro Manila showing the location of the Manila Observatory sampling site with a black rectangle.
1280 The base map shows roads, commercial centers, and major transit lines in the city. (c) Land use
1281 classification in the vicinity of the sampling site. (Sources: GADM, Snazzy Maps, OpenStreetMap,
1282 NOAA HYSPLIT, & TrajSat)

1283
1284
1285
1286
1287
1288

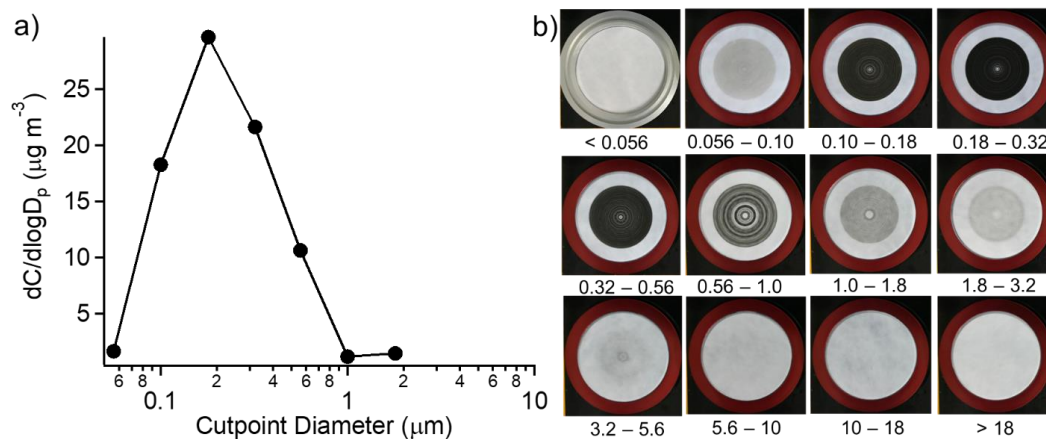


1289
1290
1291
1292
1293
1294
1295

Figure 2. Mass size distributions of total PM (blue markers) and resolved chemical species (colored bars) for MOUDI sets (a) MO3/4 and (b) MO13/14. Note that set MO13 was the single MOUDI set where BC was quantified. ICP-QQQ = sum of water-soluble elements except K; amines = sum of DMA, TMA, DEA; organic acids = sum of oxalate, succinate, adipate, pyruvate, phthalate, maleate.

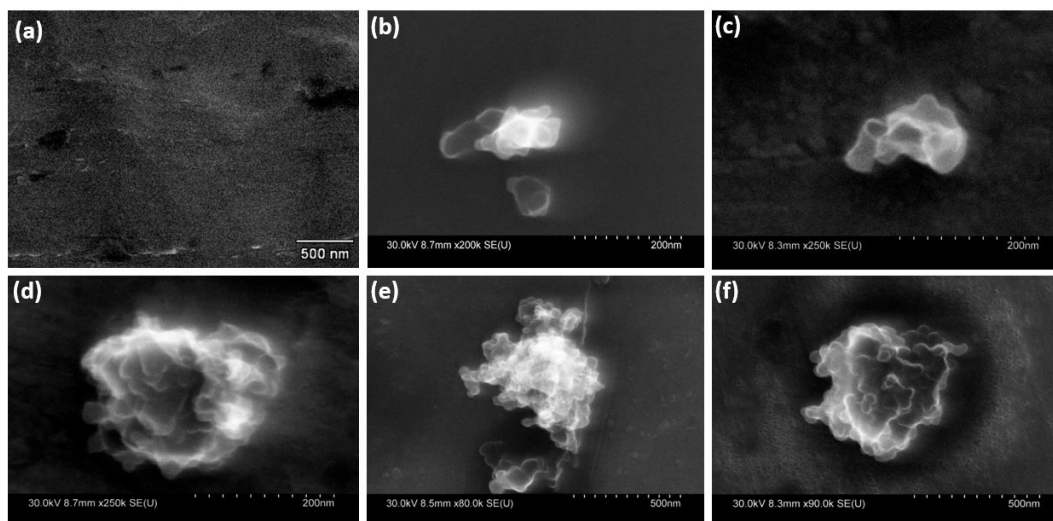


1296



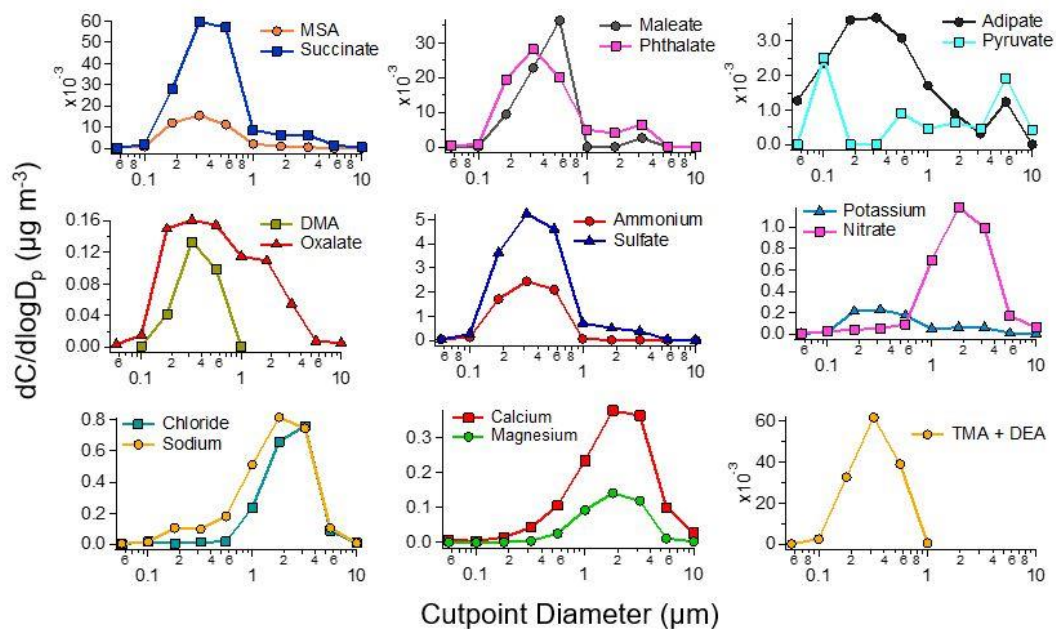
1297
1298
1299
1300
1301
1302

Figure 3. (a) Mass size distribution of BC retrieved from the MABI optical measurement at 870 nm for set MO13. Missing values were below detection limits. (b) Photographs of each stage of set MO13 with numbers below each image representing the aerodynamic diameter ranges in units of µm.



1303
1304
1305
1306
1307

Figure 4. SEM image of a (a) blank filter and (b-f) individual particles in different sub-micrometer aerodynamic diameter ranges sampled by the MOUDI: (b) 0.056–0.1 μm , (c) 0.1–0.18 μm , (d) 0.18–0.32 μm , (e) 0.32–0.56 μm , (f) 0.56–1.0 μm .

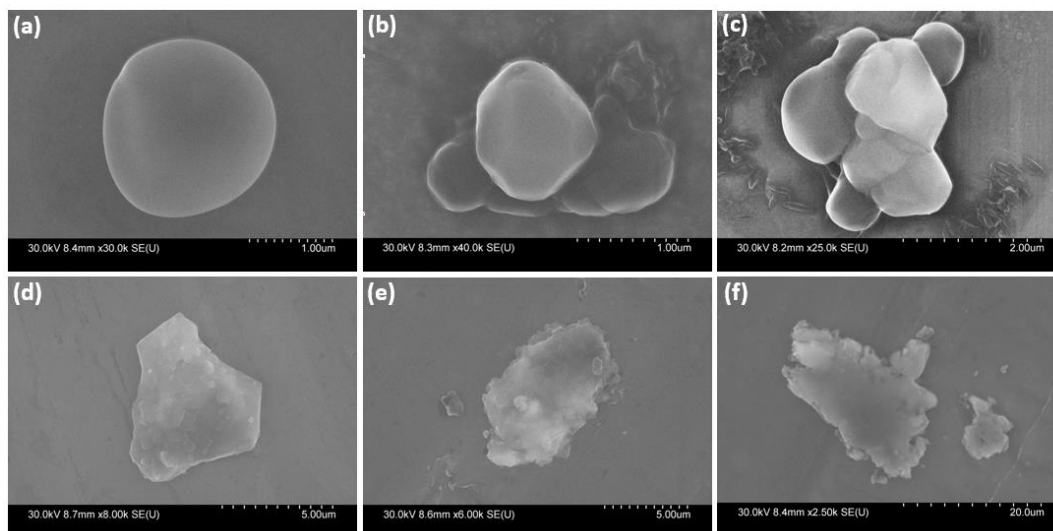


1308
1309
1310
1311

Figure 5. Average mass size distribution of water-soluble ions speciated via IC in addition to potassium from ICP-QQQ analysis.



1312



1313

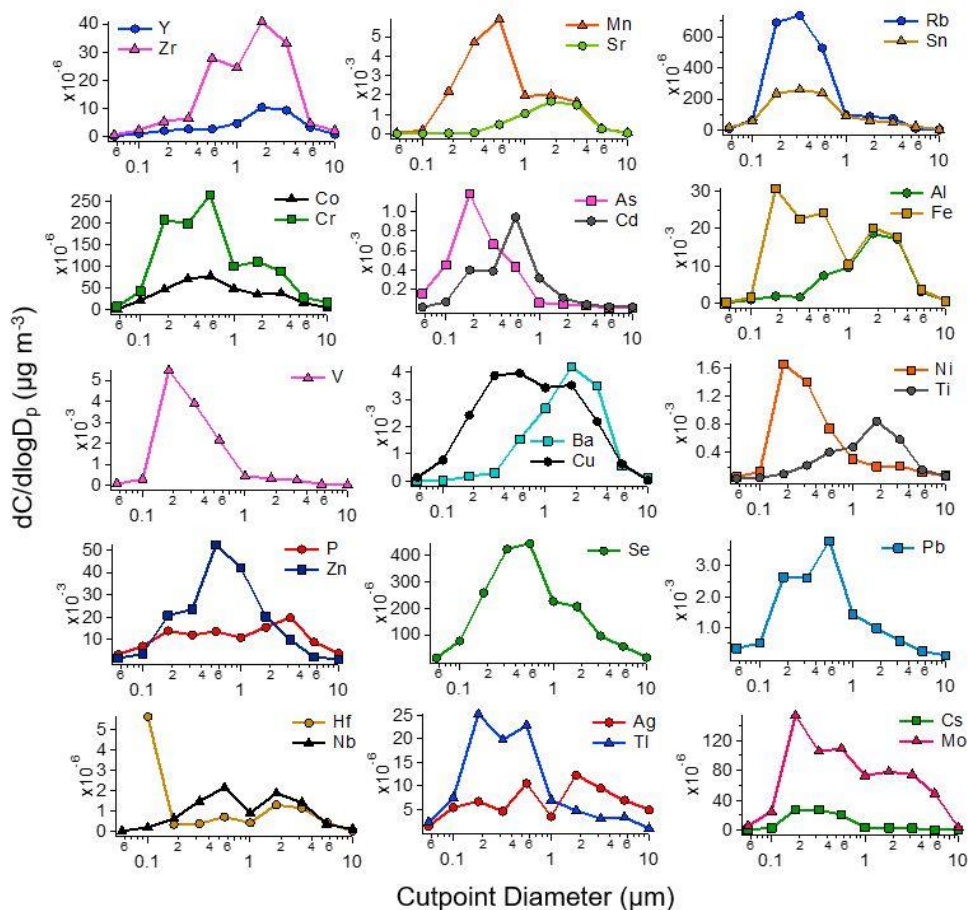
1314

1315

1316

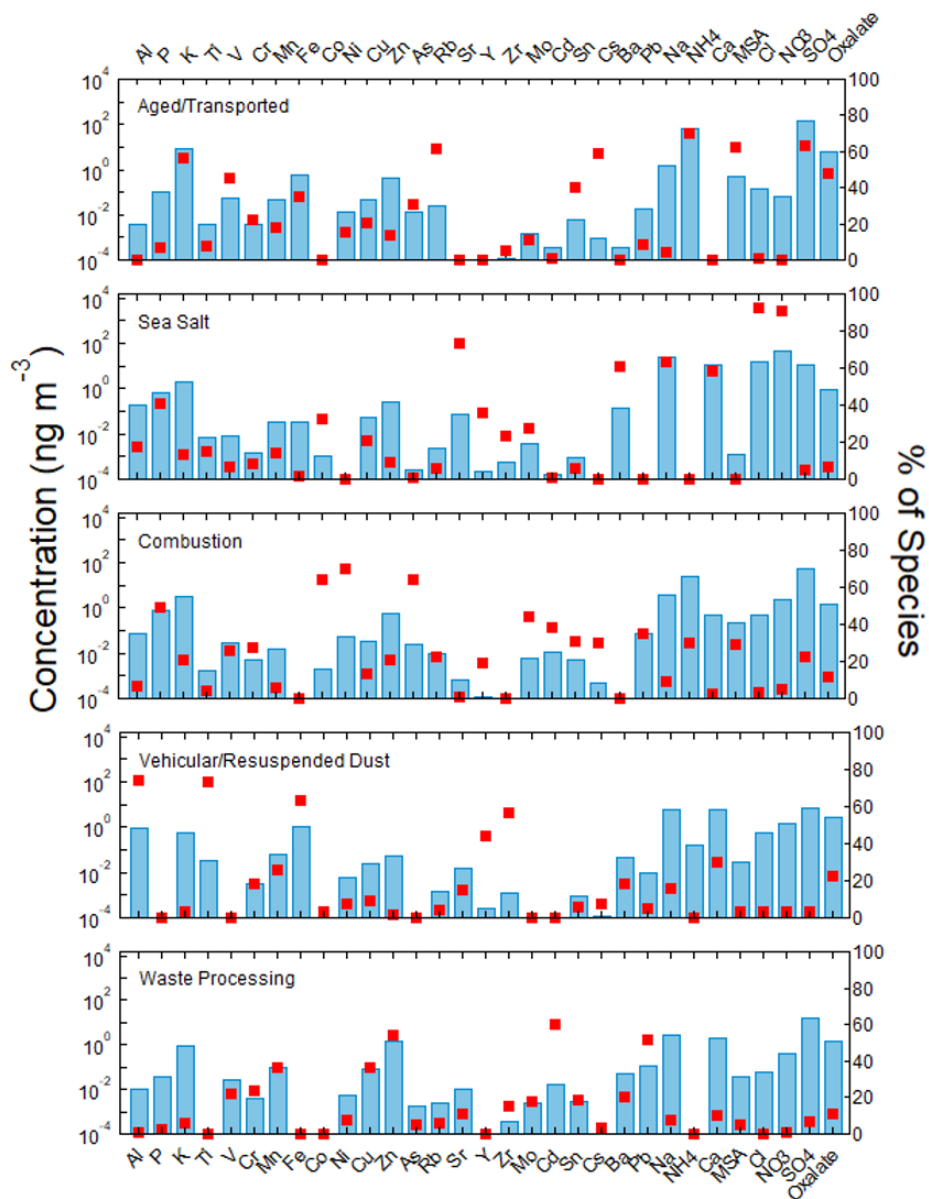
1317

Figure 6. Same as Figure 4, but for different supermicrometer aerodynamic diameter ranges sampled by the MOUDI: (a) 1.0–1.8 μm , (b) 1.8–3.2 μm ; (c) 3.2–5.6 μm , (d) 5.6–10 μm , (e) 10–18 μm , (f) > 18 μm .



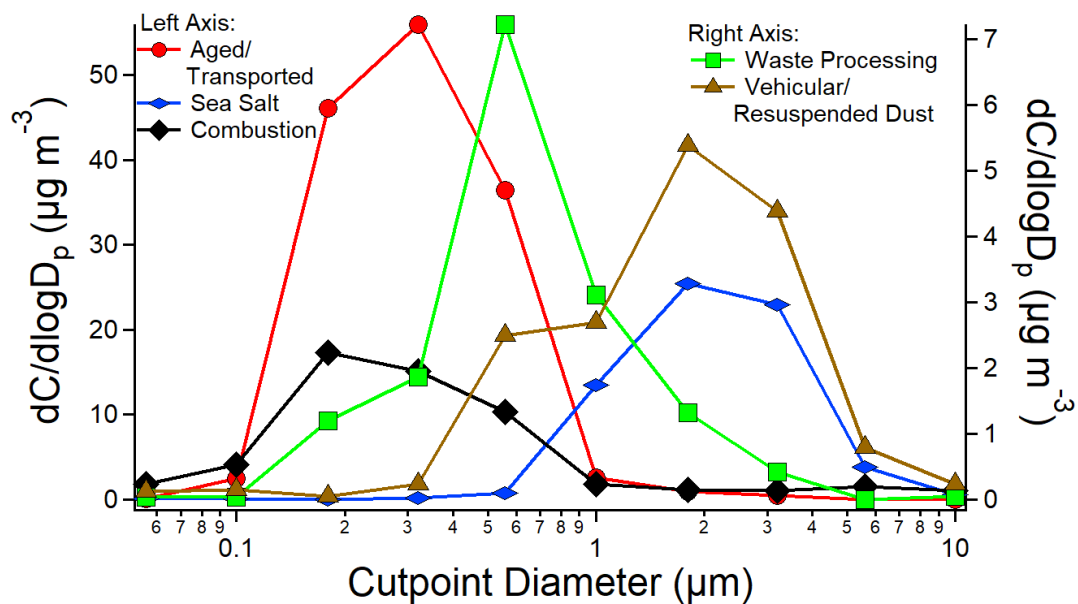
1318
1319
1320
1321

Figure 7. Average mass size distribution of water-soluble elements speciated via ICP-QQQ.



1322
 1323
 1324
 1325
 1326

Figure 8. Overview of the PMF five factor solution with blue bars representing mass concentrations and red squares signifying the percentage of mass concentration contributed to constituents by each source factor.



1327
1328
1329

Figure 9. Reconstructed mass size distributions using PMF for the five major source profiles.